

## Epitaxial effects on coherent phase diagrams of alloys

D. M. Wood and Alex Zunger

*Solar Energy Research Institute, Golden, Colorado 80401*

(Received 1 May 1989)

We present a cluster-based description of coherent binary or pseudobinary alloys and predict and contrast bulk and epitaxial composition-temperature phase diagrams and excess thermodynamic functions. This formalism addresses in a unified way phenomena characteristic of coherent epitaxial solids, including the following: for phase-separating alloys (whose constituents are insoluble in bulk below a miscibility-gap temperature), (i) epitaxial ordered phases not present in the bulk phase diagram and (ii) a stabilization of the disordered phase to far lower temperatures; and for all alloys, (iii) epitaxial changes of order-disorder transition temperatures and (iv) the pinning ("lattice latching") of the composition near where an epitaxial alloy is lattice matched to a given substrate. We illustrate these effects for  $\text{Cu}_{1-x}\text{Au}_x$ , a typical "ordering" alloy (with stable ordered compounds in bulk) and for  $\text{GaAs}_x\text{Sb}_{1-x}$ , a typical "phase-separating" alloy. Using a simple thermodynamic description of the reactions describing molecular-beam epitaxy growth of a coherent epitaxial isovalent semiconductor alloy, we demonstrate that composition pinning persists even in this growth method, and compare with available experiments.

### I. INTRODUCTION

Gradual refinements in experimental techniques now permit epitaxial growth of materials coherent with the substrate at temperatures low enough that phenomena peculiar to epitaxy occur. These effects, reviewed by Zunger and Wood,<sup>1</sup> include the following.

(i) *Epitaxial stabilization of isovalent intersemiconductor ordered compounds not present in the bulk phase diagram.* These have been observed on lattice-matched<sup>2-5</sup> (LM) or -mismatched<sup>6</sup> substrates, even when grown continuously (i.e., not layer by layer) using molecular-beam epitaxy (MBE), liquid-phase epitaxy (LPE),<sup>5</sup> and metal organic chemical-vapor deposition (MOCVD). The crystal structures observed are described in Refs. 7 and 8.

(ii) *Epitaxial selection between two competing structures for an ordered phase.* Here the crystal structure which grows epitaxially need not be the stable bulk structure, e.g., face-centered-cubic (not the stable bulk body-centered-cubic) Fe on a Cu substrate,<sup>9-11</sup>  $\alpha$ -Sn (rather than  $\beta$ -Sn) on InSb (Ref. 12) or CdTe (Ref. 13) substrates, and rocksalt (not zinc-blende) InSb on various substrates.<sup>14</sup>

(iii) *Epitaxy-enhanced solid solubility.* Here constituents insoluble in bulk below a minimum "miscibility temperature" become soluble epitaxially—even on lattice-matched substrates—at temperatures as much as 1200 °C lower, e.g., GaP-GaSb,<sup>15</sup> GaAs-GaSb,<sup>16-18</sup>  $\text{BaF}_2$ - $\text{CaF}_2$ ,<sup>19</sup> or PbS-CdS.<sup>20</sup>

(iv) *Pinning of the epitaxial alloy composition near the value lattice matched to the substrate,*<sup>18,21-26</sup> while the composition of a bulk (incoherent) alloy grown under identical conditions varies widely. This phenomenon ("lattice latching") has been observed<sup>27-30</sup> in a variety of systems on diverse substrates of various orientations in liquid-phase epitaxy growth.<sup>21-25</sup> The same effect ap-

pears in another guise in MBE growth.<sup>26</sup>

(v) Other epitaxial changes have been predicted theoretically, including shifts in order-disorder transition temperatures<sup>17</sup> and changes of bond lengths in semiconductor alloys<sup>7(a)</sup> with respect to the corresponding bulk values.

We will demonstrate that an approach which focuses on the elastic strain energy due to the epitaxial constraint satisfactorily explains these phenomena. To the extent that such a description in terms of three-dimensional equilibrium thermodynamics fails quantitatively in certain instances, kinetic and two-dimensional growth effects<sup>31,32</sup> or explicit surface effects (e.g., surface steps<sup>32,33</sup>) may be potentially important.

We begin with an elastic continuum description of a pure ordered compound and describe the phenomenon of epitaxial stabilization in Sec. II. In Sec. III we show how a pure disordered or ordered phase subject to the external constraints of bulk or epitaxial growth may be described theoretically as a mixture of clusters, and discuss the expected qualitative effects of epitaxy. In Sec. IV we give details of our computational approach for two generically typical alloy systems,  $\text{Cu}_{1-x}\text{Au}_x$  (an "ordering" alloy, i.e., with stable ordered compounds in bulk), and  $\text{GaAs}_x\text{Sb}_{1-x}$  (a "phase-separating" alloy, without stable ordered bulk compounds). In Sec. V we contrast bulk and epitaxial temperature-composition phase diagrams and give quantitative results for thermodynamic functions and microscopic cluster-related properties for these two alloys. Section VI describes composition pinning during the growth of epitaxial alloys and Sec. VII gives a thermodynamic description of molecular-beam epitaxial growth of coherent pseudobinary semiconductor alloys, where we demonstrate that composition pinning should exist even for this growth method and compare with experiment. Brief accounts of some of this work have been published.<sup>17,18</sup>

## II. CONTINUUM ELASTICITY PICTURE OF COHERENT EPITAXIAL ENERGETICS

### A. Elastic description of bulk or coherent epitaxial compounds

We begin with a brief summary of a continuum elasticity description of the strain energy of a given material under bulk and epitaxial conditions. To illustrate the principal effects we consider *cubic* systems and retain only *harmonic* terms in the energy.

Consider a face-centered-cubic (fcc) crystalline material (e.g., a zinc-blende III-V or II-VI compound) in a free-standing bulk (bk) form. Its total energy  $E_{bk}$  (per fcc site), as a function of its cubic lattice parameter  $a$ , can be expanded about the equilibrium zero-pressure value  $a_{eq}$  as

$$E_{bk}(a) = E_{eq} + \frac{9}{8}Ba_{eq}(a - a_{eq})^2 + \dots, \quad (2.1)$$

where  $E_{eq}$  is the equilibrium total energy and  $B = (C_{11} + 2C_{12})/3$  is the bulk modulus. Now consider the same cubic material grown as a thin [see Eq. (2.5)] epitaxial film on a substrate with lattice parameter  $a_s$ . Provided the lattice mismatch between the substrate and the film is accommodated *elastically*, the film is coherently strained and the lattice parameters of a unit cell parallel ( $\parallel$ ) to the substrate are determined by<sup>34</sup>  $a_s$ , while the cell dimension  $c$  normal to the substrate is free to relax. The elastic energy density  $U$  for a cubic material depends on the Cartesian strain tensor components  $\{\epsilon_{xx}, \epsilon_{yy}, \epsilon_{zz}, \epsilon_{xy}, \epsilon_{xz}, \epsilon_{yz}\}$  and the cubic elastic constants  $C_{11}$ ,  $C_{12}$ , and  $C_{44}$ . For each substrate orientation  $U$  is a quadratic form in the strains  $\epsilon_{\parallel}$  and  $\epsilon_{\perp}$  parallel and perpendicular to the substrate. The equilibrium perpendicular dimension  $c_{eq}$  is determined by setting  $dU/d\epsilon_{\perp} = 0$  for fixed  $\epsilon_{\parallel}$ ; when  $c_{eq}$  is substituted into  $U$  one finds, in analogy with Eq. (2.1), a total energy per fcc site of the coherently strained epitaxial film

$$E_{ep}(a_s, c) = E_{eq} + \frac{9}{8}qBa_{eq}(a_s - a_{eq})^2 + \frac{1}{8}Aa_{eq}[c - c_{eq}(a_s)]^2 + \dots. \quad (2.2)$$

For the principal substrate orientations  $\mathbf{G} = [001]$ ,  $\mathbf{G} = [110]$ , and  $\mathbf{G} = [111]$  the parameter  $q$ , the perpendicular elastic modulus  $A$ , and the equilibrium perpendicular dimension<sup>34</sup>  $c_{eq}(a_s)$  are related by

$$q(\mathbf{G}) = 1 - B/A(\mathbf{G}), \quad (2.3a)$$

$$c_{eq}(a_s) = a_{eq} - [3B/A(\mathbf{G}) - 1](a_s - a_{eq}). \quad (2.3b)$$

We find<sup>35,36</sup>

$$A(\mathbf{G} = [111]) = B + 4C_{44}/3, \quad (2.4a)$$

$$A(\mathbf{G} = [110]) = C_{44} + (C_{11} + C_{12})/2, \quad (2.4b)$$

$$A(\mathbf{G} = [001]) = C_{11}. \quad (2.4c)$$

According to Eq. (2.3) a coherent epitaxial film elongates perpendicular to the substrate for  $a_s < a_{eq}$  and shrinks for  $a_s > a_{eq}$ , as shown schematically in Fig. 1(a). For isotropic solids, defined by the relation  $C_{44} = (C_{11} - C_{12})/2$ ,

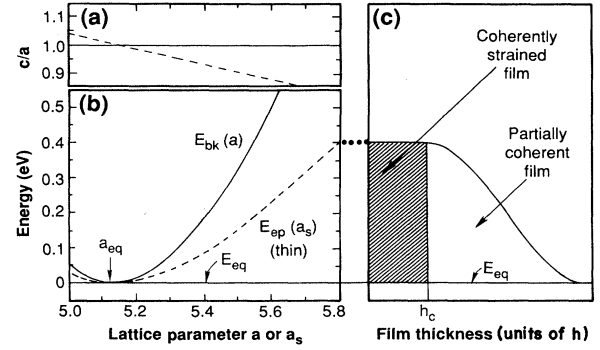


FIG. 1. Schematic dependence of strain energy of bulk and thin epitaxial material on lattice parameter  $a$  and substrate lattice parameter  $a_s$ , respectively. (b) shows tetragonal  $c/a_s$  ratio for epitaxial film; (c) shows schematic dependence of epitaxial strain energy on film thickness for fixed  $a_s$ .

$A = C_{11}$  for all three orientations. If  $c$  is unconstrained, it adopts the equilibrium value  $c_{eq}(a_s)$  and the last term in Eq. (2.2) is absent, while under hydrostatic conditions ( $a_s \rightarrow c = a$ ) we recover the bulk energy expression Eq. (2.1) for all three orientations. The “equation of state”  $E_{ep}(a_s)$  of a relaxed epitaxial film is exactly analogous to the bulk equation of state  $E_{bk}(a)$  except for the substitutions (i)  $a \rightarrow a_s$ , and (ii)  $B \rightarrow qB$ . However, the epitaxial analog of *negative* pressure is readily achieved<sup>36</sup> by the choice  $a_s > a_{eq}$ . A hydrostatically compressed bulk crystal is constrained to have  $c = a = a_s$ , so that  $E_{ep}(a_s) < E_{bk}(a = a_s)$  and  $q < 1$ . This is illustrated in Fig. 1(b), where the dashed line  $E_{ep}$  is below the solid line  $E_{bk}$  for  $a_s \neq a_{eq}$ . Thus the factor  $q$  reflects strain reduction under epitaxial (relative to hydrostatic) conditions because of the ability to perpendicularly distort. Using tabulated elastic constants<sup>37</sup> we find, e.g.,  $q[100]$ ,  $q[110]$ , and  $q[111]$  values of 0.21, 0.35, and 0.39 for CdTe; 0.36, 0.48, and 0.51 for GaSb; and 0.37, 0.48, and 0.51, respectively, for GaAs. Since for most cubic metals and semiconductors<sup>37</sup>  $C_{44}$  is larger than the isotropic value  $(C_{11} - C_{12})/2$ ,  $q[111]$  is the largest in this sequence. For very ionic materials (e.g., CsCl)  $q[100]$  is largest and  $q[111]$  smallest.

For a finite misfit  $f \equiv (a_s - a_{eq})/a_{eq}$  the epitaxial film is strained, i.e.,  $E_{ep}(a_s \neq a_{eq}) > E_{eq}$ . For thin enough films the energy is minimized if the film is *coherently strained*, i.e., its atoms are in registry with those of the substrate. When the film thickness  $h$  exceeds a critical thickness<sup>38</sup>  $h_c$  (Appendix), the strain energy of the film is minimized and reduced toward  $E_{eq}$  [shown schematically in Fig. 1(c)] by the nucleation of misfit dislocations. For  $h > h_c$  strain is shared between dislocations and elastic strain due to partial coherence with the substrate, until for  $h \gg h_c$  all coherence is lost. Within the approximations described in the Appendix, the epitaxial energy of Eq. (2.2) for  $c = c_{eq}$ , valid for  $h < h_c$ , is modified for all  $h$  to

$$E_{ep}(a_s, h) = E_{eq} + \frac{9}{8}qBa_{eq}(a_s - a_{eq})^2 S(h), \quad (2.5)$$

where

$$S(h) = \begin{cases} 1 & \text{for } h < h_c \\ \chi(2-\chi) & \text{for } h \geq h_c, \end{cases} \quad (2.6)$$

where  $\chi(h) = (h_c/h)[1 + \ln(h/b)]/[1 + \ln(h_c/b)]$  is the fraction of the misfit accommodated *elastically*, and  $b$  is the Burgers vector of the relevant misfit dislocation. Thus the total epitaxial strain energy of the partially coherent epitaxial film decays to zero with a characteristic  $1/h$  dependence for large  $h$ , as shown schematically in Figs. 1(c) and 2. In practice, activation barriers against nucleation of such dislocations in semiconductors permit coherent growth considerably beyond the equilibrium value<sup>39</sup> of  $h_c$ .

### B. Qualitative effects of epitaxy on phase stability and coexistence

To illustrate how the epitaxial constraint can selectively stabilize certain structures, consider the schematic solid-state reaction between solids  $\alpha$  and  $\beta$  to produce an ordered or disordered phase  $\alpha_x\beta_{1-x}$ :



If the reaction takes place incoherently in bulk with no applied pressure, all three species  $\alpha$ ,  $\beta$ , and  $\alpha_x\beta_{1-x}$  are free to adopt their equilibrium lattice dimensions  $a_{\text{eq}}[\alpha]$ ,  $a_{\text{eq}}[\beta]$ , and  $a_{\text{eq}}[\alpha_x\beta_{1-x}]$ , respectively (neglecting bulk coherency strain, discussed in Sec. VID). The bulk formation enthalpy is defined as the change in zero-pressure enthalpy in this reaction:

$$\Delta H_{\text{bk}}(x) = E_{\text{eq}}[\alpha_x\beta_{1-x}] - xE_{\text{eq}}[\alpha] - (1-x)E_{\text{eq}}[\beta]. \quad (2.8)$$

If, however, the reaction takes place epitaxially and all species are coherent with the substrate, the relevant change in enthalpy [from Eq. (2.2)] is the epitaxial formation enthalpy

$$\delta H_{\text{ep}}(a_s, x) = \Delta H_{\text{bk}}(x) + \Delta E_{\text{ES}}(a_s, x), \quad (2.9)$$

i.e., referred to epitaxially constrained constituents. (We will consistently label energies measured with respect to epitaxially strained constituents with a  $\delta$  and energies referred to constituents at their respective equilibria with a  $\Delta$ .) In Eq. (2.9) the excess epitaxial strain (ES) energy is

$$\Delta E_{\text{ES}}(a_s, x) = E_{\text{ES}}(\alpha_x\beta_{1-x}) - xE_{\text{ES}}(\alpha) - (1-x)E_{\text{ES}}(\beta) \quad (2.10)$$

and the epitaxial strain energy (per fcc site) for species  $\lambda$  is [Eq. (2.2)]

$$E_{\text{ES}}(\lambda) = K_\lambda (a_s - a_{\text{eq}}[\lambda])^2, \quad (2.11)$$

where  $K_\lambda = \frac{3}{8}q_\lambda B_\lambda a_{\text{eq}}[\lambda]$ .

The epitaxial stabilization effects we will discuss have their origins in the excess epitaxial strain energy  $\Delta E_{\text{ES}}(a_s)$ . Its dependence on  $a_s$  and  $q(\mathbf{G})$  can be used to manipulate the relative stabilities of bulk and epitaxial systems. Choose, for example, a substrate lattice matched to a given reaction product, e.g.,

$a_s = a_{\text{eq}}[\alpha_x\beta_{1-x}]$ . Since  $E_{\text{ES}}(\alpha_x\beta_{1-x}) = 0$  in this case,  $\Delta E_{\text{ES}}(a_s) \leq 0$  and  $\delta H_{\text{ep}}(a_s) \leq \Delta H_{\text{bk}}$ . If bulk and epitaxial entropies are similar (as we demonstrate below), the corresponding change in free energy  $F$  also obeys  $\delta F_{\text{ep}}(a_s) < \Delta F_{\text{bk}}$ , so that the reaction proceeds more completely epitaxially than in bulk. The two generic cases are  $\delta H_{\text{ep}} < 0$  and  $\delta H_{\text{ep}} > 0$ .

#### 1. $\delta H_{\text{ep}} < 0$

If  $\Delta H_{\text{bk}} > 0$  (common if  $\alpha$  and  $\beta$  are isovalent semiconductors<sup>40</sup>) but  $-\Delta E_{\text{ES}} > \Delta H_{\text{bk}}$ , one may promote a reaction epitaxially *even if it does not occur in bulk*. Case (i) is shown schematically in Fig. 2(a), whose left-hand side shows energetics of bulk and thin epitaxial films. Effect (i) of the Introduction is a manifestation of epitaxial stabilization of an ordered compound with respect to decomposition into its coherent constituents. Such an effect was predicted<sup>8(a)</sup> for a rhombohedral SiGe compound on a Si substrate,<sup>6</sup> for<sup>41,42</sup> chalcopyrite  $\text{Ga}_2\text{AsSb}$ ,  $\text{ZnHgTe}_2$ ,  $\text{GaInP}_2$ , and  $\text{ZnCdTe}_2$ , and for<sup>42</sup> CuAu-I-like  $\text{GaInP}_2$ , all on lattice-matched substrates. Epitaxial stabilization of unusual structures<sup>8,36</sup> [effect (ii) in the Introduction] may

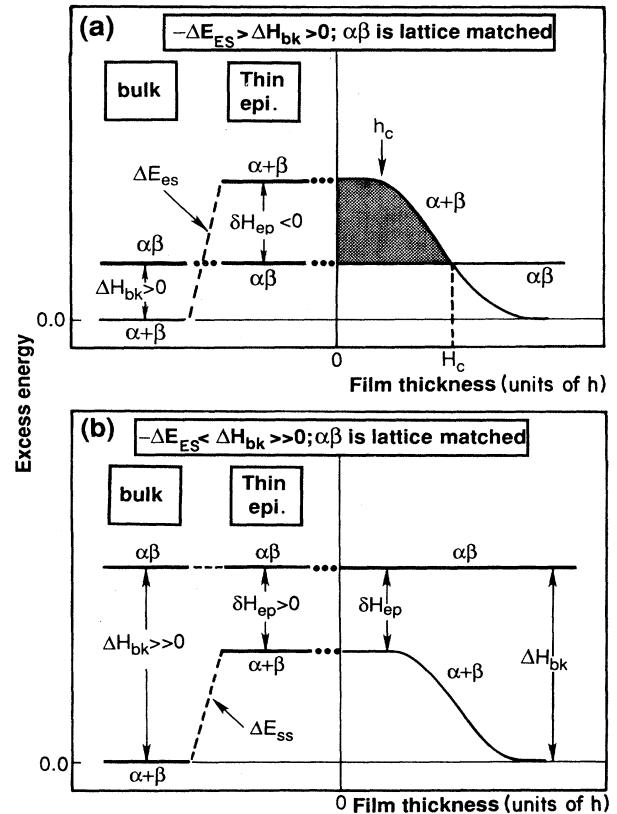


FIG. 2. Relative energies of unstable bulk alloy  $\alpha_x\beta_{1-x}$  (denoted  $\alpha\beta$ ) and constituents  $\alpha+\beta$  in bulk and epitaxially on substrate lattice matched to  $\alpha\beta$  for case where  $\alpha\beta$  is epitaxially stabilized, (a), or remains epitaxially unstable, (b). Right-hand sides indicate energy change with loss of coherence as film thickness increases.

be understood as selection of the structure with the smallest  $\delta H_{ep}$  for a given  $a_s$ , as for<sup>36</sup> CdTe in the rocksalt structure and zinc-blende MgS on substrates lattice matched to the novel (not the bulk equilibrium) phase.

The right side of Fig. 2(a) schematically shows the thickness dependence of the energies of such an epitaxially stable phase  $\alpha\beta$  and its constituents  $\alpha + \beta$  with dislocations included. Since  $\alpha\beta$  is lattice matched to the substrate, its energy is constant for all film thicknesses  $h$ ; by contrast,  $\alpha + \beta$  is strained and its energy decreases toward the unstrained value as  $h$  increases. Below the thickness  $H_c$  [shaded area in Fig. 2(a)]  $\alpha\beta$  has been epitaxially stabilized. However, as discussed by Froyen *et al.*,<sup>36</sup> once the thickness exceeds  $H_c$  even lattice-matched  $\alpha\beta$  becomes unstable towards disproportionation into lower energy constituents (with dislocations). Equation (2.5) may be applied to each epitaxially strained species to determine  $H_c$ , where epitaxial stabilization ceases. For example, consider the case  $E_{eq}[\beta] > E_{eq}[\alpha]$  but, on a substrate lattice matched to species  $\beta$ ,  $E_{ep}[\alpha] > E_{ep}[\beta] = E_{eq}[\beta]$ . Species  $\beta$  has been epitaxially stabilized with respect to  $\alpha$  provided  $h < H_c$ ; the condition  $E_{eq}[\beta] = E_{ep}[\alpha(H_c)]$  defines the  $H_c$  where such epitaxial stabilization ceases and phase  $\alpha$  resumes being the more stable. This example also illustrates the differences between the critical thicknesses  $h_c$  and  $H_c$ : note that (Appendix)  $h_c \propto a_{eq}^2[\alpha]/|\Delta a|$  while for large  $h$ ,  $H_c \propto q_\alpha B_\alpha a_{eq}^3[\alpha] \times |\Delta a| / (E_{eq}[\beta] - E_{eq}[\alpha])$ , where  $\Delta a = a_{eq}[\beta] - a_{eq}[\alpha]$ .

## 2. $\delta H_{ep} > 0$

If  $\Delta H_{bk} > 0$  is so large that  $\Delta H_{bk} + \Delta E_{ES}$  remains positive, the new critical thickness  $H_c$  does not occur, although  $0 < \delta H_{ep} < \Delta H_{bk}$  [Fig. 2(b)]. This is likely to be the case<sup>41</sup> for lattice-matched  $ABC_2$  epitaxial inter-semiconductor ordered compounds in the CuPt structure, and for disordered  $A_{1-x}B_xC$  semiconductor alloys. For such disordered alloys, as discussed in Sec. V A below, a reduction of the enthalpy will correspond to a reduction of the miscibility-gap temperature [effect (iii) of the Introduction].

In either case 1 or 2, the example above shows that the origin of epitaxial stabilization is *not* the substrate-induced strain in the  $\alpha_x\beta_{1-x}$  film (since we assumed the substrate was lattice matched to the alloy), but the epitaxial destabilization of the *constituents* [since  $E_{ES}(\alpha) + E_{ES}(\beta) > 0$ ]. The remarkable epitaxial effects noted in the Introduction are most often seen, in fact, for such lattice-matched substrates. Thus such effects must be driven by the *size mismatch*  $\Delta a$  between the *constituents*  $\alpha$  and  $\beta$  (intrinsic or "microscopic" strain), not by the strain between the  $\alpha_x\beta_{1-x}$  film and the substrate (applied or "macroscopic" strain). This becomes obvious when one assumes, for simplicity, Vegard's rule

$$a_{eq}[\alpha_x\beta_{1-x}] = xa_{eq}[\alpha] + (1-x)a_{eq}[\beta], \quad (2.12)$$

giving for  $a_s = a_{eq}[\alpha_x\beta_{1-x}]$  from Eqs. (2.10) and (2.11)

$$\Delta E_{ES}(x, a_s) = -(\Delta a)^2 x(1-x)[(1-x)K_\alpha + xK_\beta]. \quad (2.13)$$

Thus only if the *constituents* are lattice mismatched ( $\Delta a \neq 0$ ) can epitaxy alter  $\delta H_{ep}$  relative to  $\Delta H_{bk}$ .

## C. Previous interpretation of epitaxial effects

It has long been recognized that epitaxy-induced strain may modify the bulk-phase diagram of an alloy. Most work<sup>21,23,26,43-48</sup> has attempted to account for the epitaxial strain energy by adding to the bulk free energy an expression due to Jesser and Kuhlmann-Wilsdorf,<sup>49</sup>

$$E_{ES} = V_m \Gamma (a_s - a_{eq})^2 / a_{eq}^2, \quad (2.14)$$

for an epitaxial film of molar volume  $V_m$ . The elastic modulus  $\Gamma$  is variously written as  $\sigma$ ,  $2G(1+\nu)/(1-\nu)$ , or  $Y/(1-\nu)$ , where  $\nu$  is the Poisson ratio (Appendix),  $Y$  is the Young's modulus, and Eq. (2.14) is applied to an alloy by taking the elastic moduli to depend on composition in some phenomenological way. Noting that for an fcc alloy  $V_m$  is Avogadro's number  $N_A$  times the volume per fcc site  $a_{eq}^3/4$ , Eq. (2.14) is identical per fcc site to Eq. (2.2) with  $\Gamma = \frac{9}{2}qB$ .

It was frequently observed that ternary and quaternary alloys could be routinely grown at temperatures where bulk thermodynamic calculations predicted they would spinodally decompose. Quillec *et al.*<sup>47</sup> demonstrated convincingly that such stabilization for  $In_xGa_{1-x}As_yP_{1-y}$  was due to epitaxial strain by growing on a substrate so mismatched that coherent growth was impossible, and showing that below the bulk miscibility gap the alloy did indeed phase separate. Stringfellow,<sup>46</sup> following earlier work by Cahn,<sup>50</sup> examined stability of bulk alloys in the presence of "coherency strain" (Sec. VI D) associated with the rise in strain energy upon decomposition of an alloy whose lattice parameter depends on composition. Using a term identical to Eq. (2.14) he predicted very large depressions of miscibility-gap temperatures for semiconductor alloys with large  $\Delta a$ ; similar analyses have been given by Quillec *et al.*<sup>23</sup> and Ishikawa and Ito.<sup>48</sup>

Recent theoretical work clarifies how ordered compounds may be epitaxially stabilized,<sup>7,8,36,51</sup> the thermodynamics of and phase equilibrium among stressed solids,<sup>29,52,53</sup> and the nature of the structural phase transitions possible. Coherent epitaxial effects on liquid-phase epitaxy<sup>54</sup> have been examined by Larché and Cahn<sup>29</sup> and by Kuznetsov *et al.*<sup>55</sup> Other recent theoretical work treats inhomogeneous epitaxial film relaxation,<sup>56,57</sup> Bruinsma and Zangwill<sup>58</sup> have used a phenomenological description to understand and classify modes of epitaxial growth based on wetting<sup>58(a)</sup> and have examined stabilization of metastable phases in epitaxial overlayers.<sup>58(b)</sup> Gilmer and Grabow<sup>59</sup> have used molecular dynamics and model potentials to understand such growth modes.

The complete response of an alloy to the epitaxial constraint is most conveniently displayed as a composition-temperature ( $x, T$ ) phase diagram. We turn next to a description of a methodology which can describe a bulk or epitaxial alloy in any state of order.

### III. CLUSTER DESCRIPTION OF BULK AND EPITAXIAL ALLOYS

#### A. Limitations of a continuum description

A variety of phenomena may occur in phase diagrams of binary alloys, including ordered or disordered single phases, regions of two-phase coexistence, and triple points. Because of the absence of microscopic configurational degrees of freedom ( $2^N$  different arrangements of  $A$  and  $B$  atoms among  $N$  lattice sites) in phenomenological alloy treatments, they fail (1) in describing properties of ordered phases, and (2) in describing coexistence between phases.

First, a continuum description inevitably fails at temperatures low enough that *ordering* occurs. Ordered compounds directly manifest the microscopic nature of the structural units of the alloy, since ordered crystals may be described by a periodically repeated local atomic arrangement ("cluster") or unit cell. Microscopic configurations of  $A$  and  $B$  atoms—even if they share the same *elastic* properties—may be *chemically* very different and hence have different values of  $E_{\text{eq}}$  in Eq. (2.1). The two alloy systems  $\text{Cu}_{1-x}\text{Au}_x$  and  $\text{GaAs}_x\text{Sb}_{1-x}$  discussed extensively below share a similar lattice mismatch between the constituents ( $\sim 0.46$  and  $0.43$  Å for Cu-Au and GaAs-GaSb, respectively) and are elastically qualitatively similar (see Tables I and II below). They are nonetheless strikingly different: the former exhibits stable ordered compounds in bulk, while the latter does not. These chemical effects contribute significantly to the alloy excess energy [included in  $E_{\text{eq}}$  of Eqs. (2.1) and (2.2)] and entropy and are beyond the scope of a continuum treatment.

Second, an elastic continuum description using, e.g., Eq. (2.14) cannot treat phase *coexistence* because it cannot readily distinguish between the energies of two different phases of the same composition at the same temperature. Configurational degrees of freedom constitute additional channels for achieving thermodynamic equilibrium and affect phase boundaries, e.g., order-disorder transition temperatures. For example, the disordering reaction of an ordered  $AB$  compound  $AB \rightarrow A_{0.5}B_{0.5}$  may be achieved by a variety of local environments all consistent with a macroscopic alloy composition  $x=0.5$ ,

TABLE I. Bulk formation enthalpy  $\Delta H$  (kcal/fcc-site mol), equilibrium lattice parameter  $a_{\text{eq}}$  (Å), and cubic elastic constants (GPa) for  $\text{Cu}_{4-n}\text{Au}_n$  ordered compounds. These are used with an alloy-induced cluster relaxation parameter  $K=0.20772$ ; see Refs. 60(c) and 67. Values for  $n=0,4$  from fcc structures, for  $n=1,3$  from  $\text{Cu}_3\text{Au}$  structure, for  $n=2$  from  $\text{CuAu-I}$  structure.

	$\Delta H$	$a_{\text{eq}}$	$C_{11}$	$C_{12}$
Cu	0.0	3.6148	169.9	122.6
$\text{Cu}_3\text{Au}$	-1.556	3.7426	176.7	133.7
$\text{CuAu-I}$	-2.100	3.8659	188.3	150.3
$\text{CuAu}_3$	-1.373	3.9820	194.0	158.0
Au	0.0	4.0784	190.0	161.0

e.g., 100%  $A_2B_2$  clusters, or equal proportions of ( $A_3B + AB_3$ ) or ( $A_4 + B_4$ ). Continuum descriptions fail to acknowledge the central role of temperature in controlling cluster populations even though, since these clusters have different properties, the macroscopic alloy energy depends very much on their relative proportions.

To the extent that relevant cluster-cluster interactions are effectively weak (or that long-range interactions simply renormalize shorter-range intracenter interactions<sup>60(a)</sup>), even the nearest-neighbor  $A_{4-n}B_n$  ( $n=0-4$ ) clusters present in an fcc  $A_{1-x}B_x$  alloy can be used as the structural units to describe the corresponding ordered compound  $A_{4-n}B_n$ . It is natural, therefore, to describe a disordered alloy as a mixture of such clusters, whose proportions depend on the alloy composition  $x$  and temperature  $T$  and are determined so as to minimize the alloy free energy for  $(x, T)$ . Such an approach permits calculation<sup>60</sup> of the energy and entropy for all of the possible states of order spanned by the clusters. Using parallel tangent constructions, regions of phase coexistence may be determined and hence the entire  $(x, T)$  phase diagram may be computed. The details of such an approach are deferred to Sec. IV.

#### B. Application of alloy constraints to clusters

The constraints of bulk or coherent epitaxial growth of a *pure ordered compound* are well understood (Sec. II A), and we describe next how these constraints may be applied correctly to the constituent clusters making up an arbitrary *alloy* phase. Consider<sup>60(a)</sup> the  $2^N$  possible configurations of  $A$  and  $B$  atoms on a lattice of  $N$  points. We may characterize each configuration  $\sigma$  by its excess energy  $\Delta E(\sigma, \phi)$ , referred to an equivalent number of  $A$  and  $B$  atoms in their respective pure equilibrium environments. Here  $\phi$  is the physically relevant structural parameter, e.g., the lattice parameter  $a$  for a bulk alloy, and for an epitaxial alloy on a fixed substrate, the perpendicular dimension  $c$  [Eqs. (2.1) and (2.2)]. An alloy of fixed composition  $x$  at temperature  $T$  can occur as various phases  $\gamma$ , e.g., an ordered structure or a disordered phase, each characterized by an ensemble average  $\langle \Delta E(\sigma, \phi) \rangle_\gamma$  over the configurations  $\sigma$  occurring in phase  $\gamma$ . Rather than evaluate the  $2^N$  values of  $\Delta E(\sigma, \phi)$ , one may expand each configuration in terms of elementary figures  $m$  (sites, pairs, triangles, tetrahedra, . . .) each with associated interaction energies  $J_m(\phi)$  (including up to  $m$ -body interactions) within figure  $m$ ,

$$\Delta E(\sigma, \phi) = N \sum_{m=1}^M \bar{\pi}_m(\sigma) J_m(\phi), \quad (3.1)$$

where  $\bar{\pi}_m(\sigma)$  is the lattice-average correlation function for figure  $m$  in configuration  $\sigma$ . This is the first of two key approximations: (1) we will include only figures of a finite maximum size  $M$ , assuming the series to be rapidly convergent. In the cluster variation method we make the second key approximation, (2) retaining statistical correlations only up to figures of size  $M'$ . Below we will take  $M=M'$  and work in the nearest-neighbor approximation, with the figures for a binary alloy corresponding to the

TABLE II. Bulk formation enthalpy  $\Delta H$  (kcal/fcc-site mol), equilibrium lattice parameter  $a_{\text{eq}}$  (Å), and cubic elastic constants (GPa) for  $\text{Ga}_4\text{As}_{4-n}\text{Sb}_n$  ordered compounds. Values for  $n=0,4$  from zincblende structure, for  $n=1,3$  from luzonite structure, and for  $n=2$  from CuAu-I-like structure: I and II indicate, respectively, VFF and LAPW results described in text.

	$\Delta H(\text{I})$	$\Delta H(\text{II})$	$a_{\text{eq}}$	$C_{11}$	$C_{12}$
GaSb	0.0	0.0	6.1068	82.147	37.377
$\text{Ga}_4\text{AsSb}_3$	0.619	1.01	5.9891	89.138	41.381
$\text{Ga}_2\text{AsSb}$	0.870	1.33	5.8786	96.373	45.864
$\text{Ga}_4\text{As}_3\text{Sb}$	0.681	1.15	5.7759	103.789	50.855
GaAs	0.0	0.0	5.6816	111.177	56.311

five  $A_{4-n}B_n$  tetrahedra with  $n=0-4$ . Longer-range interactions are treated in Ref. 60(a).

To calculate the interaction energies  $J_m(\phi)$  we note that although  $\bar{\pi}_m(\sigma)$  for an *arbitrary* configuration  $\sigma$  is unknown, for simple states of order, e.g., periodic crystals  $\sigma=n$  whose repeat units are the figures of size  $M$ , the  $\bar{\pi}_m$  are simple geometrical constants.<sup>60,61</sup> Thus the excess energy of such a periodic structure (e.g.,  $A_{4-n}B_n$  crystals) is

$$\Delta E(n, \phi) = N \sum_{m=1}^M \bar{\pi}_m(n) J_m(\phi). \quad (3.2)$$

If the  $M$  equations of state  $\{\Delta E(n, \phi)\}$  for the  $M$  linearly independent ordered structures are known, we can evaluate the  $M$  functions

$$J_m(\phi) = \frac{1}{N} \sum_{n=1}^M [\bar{\pi}_m(n)]^{-1} \Delta E(n, \phi). \quad (3.3)$$

Substituting into Eq. (3.1), we find

$$\Delta E(\sigma, \phi) = \sum_n \xi_n(\sigma) \Delta E(n, \phi), \quad (3.4)$$

where

$$\xi_n(\sigma) = \sum_{m=1}^M \bar{\pi}_m(\sigma) [\bar{\pi}_m(n)]^{-1} \quad (3.5)$$

and  $\xi_n(\sigma)$  is now the occurrence frequency of figure  $n$  in configuration  $\sigma$ . With these approximations the relevant configurational average  $P_n(\gamma, x, T) = \langle \xi_n(\sigma) \rangle_\gamma$  can be calculated simply.<sup>60(a)</sup> Thus this analysis demonstrates that the ensemble average of the *alloy* energy may be interpreted as a statistical average over the energies of *ordered structures*  $n$ ; for phase  $\gamma$ ,

$$\Delta E_\gamma(x, T) = \langle \Delta E(\sigma, \phi) \rangle_\gamma = \sum_{n=1}^M P_n(\gamma, x, T) \Delta E(n, \phi). \quad (3.6)$$

The equilibrium energy for phase  $\gamma$  is found by seeking the  $\{P_n\}$  which minimize the free energy; the equilibrium value of the structural variable  $\phi$  is found by minimizing  $\Delta E$  with respect to  $\phi$ .

### C. Macroscopic alloy properties

The formalism in the previous section permits us to use a representation in which an alloy (ordered or disordered)

is spanned by constituent clusters whose energies are taken from ordered compounds,<sup>60,61</sup> each subject to the same constraint. For a *bulk* alloy, it is that the lattice parameter  $a$  be the equilibrium value for the alloy. We will characterize each constrained ordered compound  $n$  by its excess energy function  $\Delta E^{(n)}(a)$  [ $\Delta E(n, \phi)$  of Eq. (3.2)]; at its own equilibrium lattice parameter  $a_{\text{eq}}^{(n)}$  (denoted  $a_n$  below) its energy  $\Delta E^{(n)}$  coincides with its formation enthalpy  $\Delta H^{(n)}$  at zero pressure. For an  $A_{1-x}B_x$  alloy in bulk (bk) form at zero pressure Eq. (3.6) gives

$$\Delta H_{\text{bk}}(x, T) = \sum_n P_n(x, T) \Delta E_{\text{bk}}^{(n)}[a_{\text{eq}}(x, T)], \quad (3.7)$$

where  $P_n$  is the probability of cluster  $n$  in the bulk alloy at  $(x, T)$ . We determine the bulk equilibrium lattice parameter  $a_{\text{eq}}(x, T)$  for zero applied pressure by the requirement  $d\Delta H_{\text{bk}}(x, T)/da = 0$ . Since in general  $a_{\text{eq}}(x, T)$  differs from  $a_n$ , *the individual clusters in the alloy environment are strained*.

To treat epitaxial alloys we assume the substrate is thick in comparison to the epitaxial film (so that<sup>29</sup> the film may be taken as homogeneous) and that the film thickness  $h$  satisfies (monolayer)  $\ll h < h_c(x)$ , so that surface energies are thermodynamically negligible and strain is accommodated elastically. Under coherent epitaxial conditions each ordered compound (cluster  $n$ ) is subject to the external constraint  $a_{\parallel} = a_s$  and  $c = c_{\text{eq}}(a_s, x, T)$ , so that

$$\Delta H_{\text{ep}}(a_s, x, T) = \sum_n \bar{P}_n(a_s, x, T) \Delta E_{\text{ep}}^{(n)}[a_s, c_{\text{eq}}(a_s, x, T)], \quad (3.8)$$

where  $\bar{P}_n$  is evaluated for the epitaxial alloy and  $c_{\text{eq}}(a_s, x, T)$  is the equilibrium dimension perpendicular to the substrate, determined via  $d\Delta H_{\text{ep}}(a_s, x, T)/dc = 0$ . This approach differs from another recent cluster-based treatment,<sup>62</sup> in which the condition  $d\Delta E_{\text{ep}}^{(n)}/dc = 0$  was incorrectly imposed for each cluster, rather than for the alloy.

The energy of an ordered compound subject to the bulk or epitaxial constraint may be calculated from first principles.<sup>8,36,41,60(c),60(d)</sup> For small deformations it may be conveniently described by harmonic elasticity theory<sup>7</sup> (as justified in Sec. IV C and Fig. 3 below). Per fcc site for bulk and epitaxial clusters we use Eqs. (2.1) and (2.2), respectively:

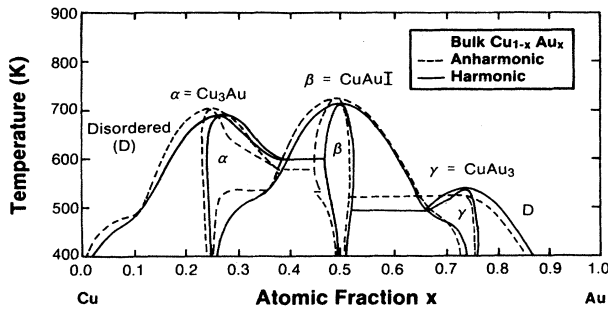


FIG. 3. Phase diagram of bulk  $\text{Cu}_{1-x}\text{Au}_x$ : using harmonic (solid) and anharmonic Murnaghan (dashed) equations of state.

$$\Delta E_{\text{bk}}^{(n)}(a) = \Delta H_n + \frac{9}{8} a_n B_n (a - a_n)^2, \quad (3.9a)$$

$$\Delta E_{\text{ep}}^{(n)}(a_s, c) = \Delta H_n + \frac{9}{8} a_n q_n B_n (a_s - a_n)^2 + \frac{1}{8} a_n A_n [c - c_{\text{eq}}^{(n)}(a_s)]^2, \quad (3.9b)$$

where  $\Delta H_n$ ,  $B_n$ , and  $a_n$  are the formation enthalpy, bulk modulus, and equilibrium lattice parameter, respectively, of the ordered compound from which cluster  $n$  is drawn. The parameters  $A_n$ ,  $c_{\text{eq}}^{(n)}(a_s)$ , and  $q_n$  are given in Eqs. (2.3) and (2.4), where the cluster index  $n$  is absent.

There are simple relationships between macroscopic properties of bulk and epitaxial alloys within the harmonic approximation if the normalized epitaxial cluster probabilities  $\{\tilde{P}_n(x, T)\}$  are known. First, using the explicit expression for  $c_{\text{eq}}(a_s)$  given in Eq. (2.3b) for each  $n$ ,

$$c_{\text{eq}}(a_s, x, T) = a_{\text{eq}}(x, T) - (3Q/R - 1)[a_s - a_{\text{eq}}(x, T)], \quad (3.10)$$

where

$$a_{\text{eq}}(x, T) = \frac{1}{Q} \sum_n \tilde{P}_n(x, T) B_n a_n^2 \quad (3.11)$$

and

$$Q(x, T) = \sum_n \tilde{P}_n(x, T) a_n B_n, \quad (3.12)$$

$$R(x, T) = \sum_n \tilde{P}_n(x, T) a_n A_n. \quad (3.13)$$

To derive the relationship between epitaxial and bulk alloy enthalpies, substitute Eq. (2.3b) for  $c_{\text{eq}}^{(n)}(a_s)$  into Eq. (3.9b), substitute Eq. (3.9b) into Eq. (3.8), and write the epitaxial alloy energy as a quadratic in terms of  $(c_{\text{eq}}^{(n)} - a_n)^2$ ,  $(a_s - a_n)^2$ , and  $(c_{\text{eq}}^{(n)} - a_n)(a_s - a_n)$ . One then substitutes Eq. (3.10) for  $c_{\text{eq}}$ , performs the sums using the definitions in Eqs. (3.12) and (3.13), and completes squares to form terms in  $[a_s - a_{\text{eq}}(x, T)]^2$  and  $[a_{\text{eq}}(x, T) - a_n]^2$  to find for any of the three principal orientations per fcc site

$$\begin{aligned} \Delta H_{\text{ep}}(a_s, x, T) &= \Delta H_{\text{bk}}(x, T) + \frac{9}{8} a_{\text{eq}}(x, T) q(x, T) B(x, T) \\ &\quad \times [a_s - a_{\text{eq}}(x, T)]^2 \\ &= \Delta H_{\text{bk}}(x, T) + E_{\text{ES}}(a_s, x, T), \end{aligned} \quad (3.14)$$

where

$$B(x, T) = Q(x, T) / a_{\text{eq}}(x, T), \quad (3.15a)$$

$$q(x, T) = 1 - Q(x, T) / R(x, T), \quad (3.15b)$$

and  $\Delta H_{\text{bk}}$  is given in Eq. (3.7). These quantities are evaluated using the *epitaxial* cluster probabilities  $\{\tilde{P}_n(x, T)\}$  for a particular value of  $a_s$ . The second term in Eq. (3.14) is precisely of the *form* expected for an alloy described as an elastic continuum with elastic moduli

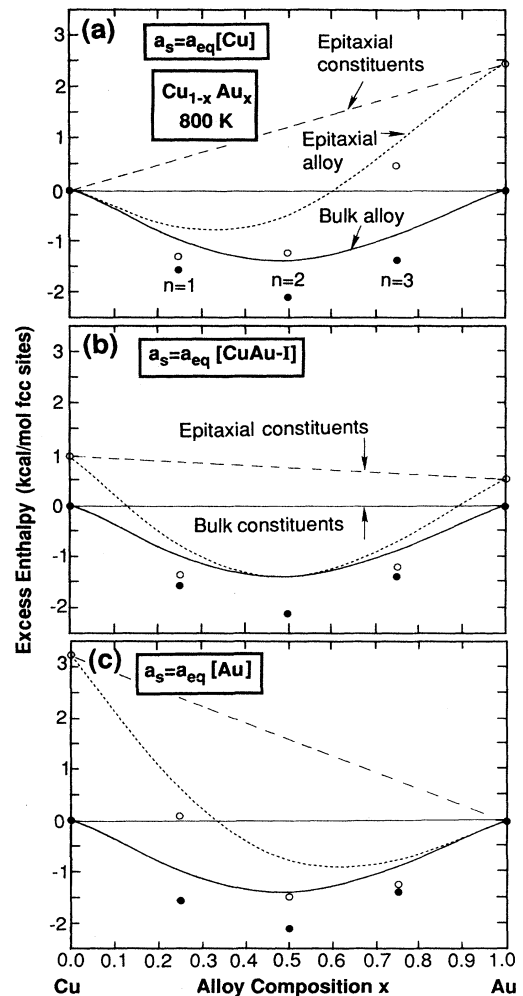


FIG. 4. Excess enthalpies of bulk and epitaxial  $\text{Cu}_{1-x}\text{Au}_x$  alloys on [001] substrates for  $a_s = a_{\text{eq}}[\text{Cu}]$ ,  $a_{\text{eq}}[\text{CuAu-I}]$ , and  $a_{\text{eq}}[\text{Au}]$ , (a), (b), and (c), respectively. Solid (open) circles indicate  $T=0$  values for bulk (epitaxial) ordered compounds. Solid (fine dashed) lines indicate mixing enthalpies of disordered bulk (epitaxial) alloy. Coarse dashed lines indicate energy of equivalent amounts of epitaxial constituents.

which depend on  $(x, T)$  [see Eqs. (2.14) and (2.2)]. However, Eqs. (3.10)–(3.15) permit explicit calculation of the alloy structural parameters  $a_{\text{eq}}(x, T)$ ,  $c_{\text{eq}}(a_s, x, T)$ ,  $B(x, T)$ , and  $q(x, T)$  from cluster properties [while Eq. (2.14) gives no such prescription], thus placing phenomenological elastic treatments of alloys on a microscopic footing.

Provided the cluster probabilities are known, Eqs. (3.7)–(3.15) provide a complete, consistent microscopic description of bulk and epitaxial phase diagrams; we defer to Sec. IV a description of how the  $\{\tilde{P}_n(x, T)\}$  are found in practice. Independent of these details, we note the following.

(i) When  $a_s = a_{\text{eq}}(x, T)$  there is no epitaxial strain energy and no tetragonal deformation of the alloy. Since the cluster probabilities for a specified phase are determined by minimizing its free energy at  $(x, T)$ , the epitaxial cluster probabilities  $\{\tilde{P}_n\}$  are identical to the bulk values  $\{P_n\}$  under these conditions. Hence the energy and structural properties of a given bulk alloy phase (either ordered or disordered) are indistinguishable from those of the epitaxial alloy on a lattice-matched substrate.

(ii) Coexistence between *different* phases (phase boundaries, miscibility gaps, order-disorder transitions) can change even on substrates lattice matched to the alloy, however. Miscibility gaps (regions of the phase diagram where a homogeneous alloy is unachievable) are associated with regions where  $d^2\Delta F/dx^2 < 0$ , where  $\Delta F = \Delta H - T\Delta S$  is the alloy free energy of mixing. For coherent epitaxy there is a positive contribution to  $d^2\Delta H/dx^2$  (with respect to bulk) from  $E_{\text{ES}}$  [second term in Eq. (3.14)]; see Sec. VI A and Figs. 4–6.

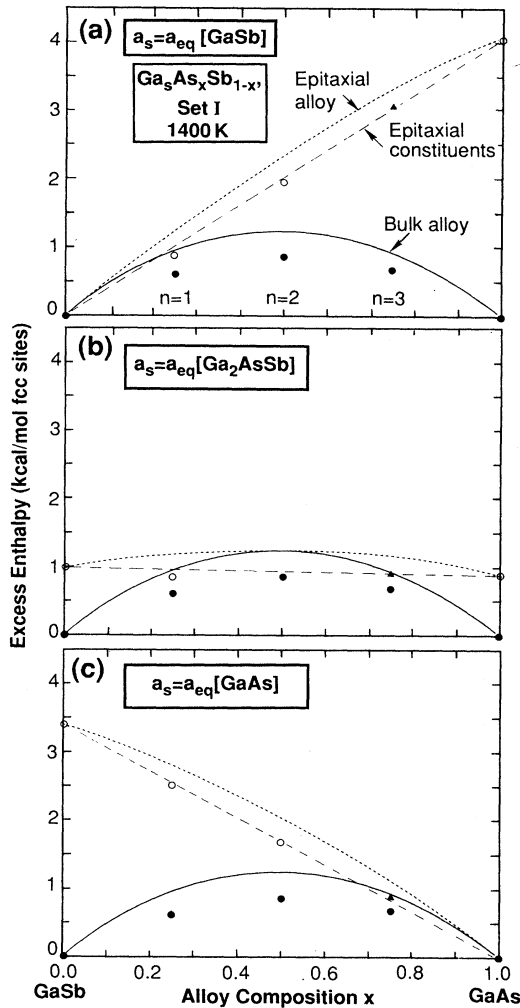


FIG. 5. Excess enthalpies using model I data (Table II) of bulk and epitaxial  $\text{GaAs}_x\text{Sb}_{1-x}$  alloys on [001] substrates for  $a_s = a_{\text{eq}}[\text{GaSb}]$ ,  $a_{\text{eq}}[\text{Ga}_2\text{AsSb}]$ , and  $a_{\text{eq}}[\text{GaAs}]$ , (a), (b), and (c), respectively. Solid (open) circles indicate  $T=0$  values for bulk (epitaxial) ordered compounds. Solid (fine dashed) lines indicate mixing enthalpies of disordered bulk (epitaxial) alloy. Solid triangles indicate epitaxially unstable ordered compounds; coarse dashed lines indicate energy of epitaxial constituents.

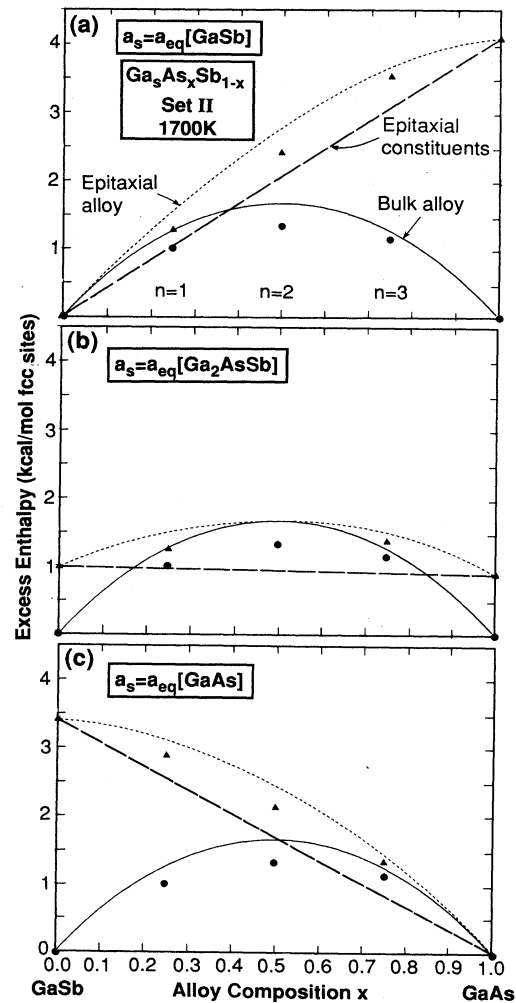


FIG. 6. Same as for Fig. 5, but using model II data (Table II) for  $\text{Ga}_4\text{As}_{4-n}\text{Sb}_n$  ordered compounds.

(iii) The cluster approach can readily distinguish among competing phases at  $(x, T)$  on the basis of the different statistical and structural properties of each phase. For alloys of lattice-mismatched constituents we expect simple trends in the relative energies of ordered compounds and disordered alloys (bulk or epitaxial). For example, at  $T=0$  we note that for an ordered compound  $m$ ,  $P_n = \delta_{n,m}$  and Eq. (3.7) [(3.8)] reverts to Eq. (3.9a) [3.9b], except that the last terms in Eqs. (3.9)—due to distortions because a cluster is embedded in an alloy environment—vanish for ordered compounds. Disordered alloys (for which these are important, since  $P_n \neq \delta_{n,m}$ ) could thus have higher strain energies than ordered compounds of the same composition (see Figs. 4–6 below), making possible metastable long-range ordering. At finite temperatures  $-T\Delta S$  may make the free energy  $\Delta F$  lower for a disordered phase than for the ordered compound, leading to an order-disorder transition temperature.

#### D. Limitations of three-dimensional thermodynamic description

Our description of a bulk or epitaxial alloy is based on clusters embedded in a *three-dimensional* homogeneous medium, with energies which do not depend, e.g., on the distance of the cluster from the surface of a growing alloy. Most thin-film growth techniques, however, are characterized by growth at a *free surface*, with (i) high surface atomic mobilities but far lower (bulklike) mobilities for “buried” atoms a few monolayers below, and (ii) extrinsic surface defects or intrinsic features such as surface steps.

Regarding (i), it is likely that the energy of a cluster depends on whether it is at a surface (with reduced coordination and reduced strain) or inside the film (with strain uniform above and below the cluster). Thus the atomic arrangement (including surface reconstruction) which minimizes the free energy of a two-dimensional *surface* layer may differ from the corresponding *three-dimensional* configuration. Such surface-ordered arrangements may be “frozen in” at the growth temperature (usually greater than the three-dimensional equilibrium ordering temperature) because of the low mobility after they are buried by the next layer. A postgrowth anneal at somewhat higher temperatures will eventually cause reversion to the three-dimensional equilibrium disordered phase. Hence order-disorder transition temperatures in a strictly three-dimensional description form a *lower limit* to ordering temperatures for systems for which the surface free energy during growth is important. Provided three-dimensional equilibrium is achieved, our analysis should be valid for films more than a few monolayers thick.

Regarding item (ii), we explicitly neglect effects due to the existence of surface steps. Suzuki *et al.*,<sup>32</sup> Bellon *et al.*,<sup>63</sup> and Van Vechten<sup>64</sup> have noted that different surface migration rates for atoms adsorbed on exposed steps<sup>32,33</sup> and step-related changes in reactivity may affect the observed structure of a growing film if it is kinetically limited. Such effects should be modeled by *kinetic* simu-

lations (Monte Carlo<sup>65</sup> or molecular-dynamics<sup>59,66</sup>) and are outside the scope of our thermodynamic treatment. The presence of a free surface or surface steps may even catalyze ordering into structures not expected to be stable. Lattice-mismatched isovalent  $A_{1-x}B_xC$  semiconductor alloys (e.g.,  $\text{GaAs}_x\text{Sb}_{1-x}$ ) are most commonly observed<sup>2</sup> to order into a rhombohedral CuPt-like ternary compound at  $x=0.5$ . Bernard *et al.*<sup>41</sup> have calculated that  $\Delta H_{\text{bk}} > 0$  and  $\delta H_{\text{ep}} > 0$  for CuPt  $\text{Ga}_2\text{AsSb}$ , so that *neither* bulk nor epitaxial ordering is expected on the basis of three-dimensional thermodynamics; this is probably true for other  $A_{1-x}B_xC$  alloys. Suzuki *et al.*<sup>32</sup> and Bellon *et al.*<sup>63</sup> have proposed mechanisms for propagation of CuPt ordering based on surface-mediated effects.

Our formalism is hence most appropriate for describing near-equilibrium three-dimensional growth, e.g., by liquid-phase epitaxy (for which famatinitite ordering has been observed<sup>5</sup>).

#### IV. INGREDIENTS OF QUANTITATIVE CALCULATIONS

The results of Sec. III are general alloy properties which do not depend on the particular number of clusters retained or the values of the (normalized) cluster probabilities. Given  $\{\Delta H_n, a_n, C_{11}^{(n)}, C_{12}^{(n)}, C_{44}^{(n)}\}$  for all relevant clusters  $n$ , the cluster probabilities  $\{P_n(x, T)\}$ , the entropy  $S$ , and hence the free energy  $F$  for each possible phase can be determined. Using parallel tangent constructions we may hence calculate the complete  $(x, T)$  phase diagram.

##### A. Source of cluster equations of state

###### 1. $\text{Cu}_{1-x}\text{Au}_x$

The description of Sec. III B requires selection of ordered periodic structures whose equations of state  $\Delta E^{(n)}(\phi)$  as a function of the structural parameter  $\phi$  determine the interactions in the alloy system. It is natural to select ordered compounds which are candidate low-temperature stable structures for the fcc-based alloys we consider. One may use the structures satisfying the Landau-Lifshitz criteria (Refs. 7 and 8 and references therein), such that (i) the space group of the ordered structure is a subgroup of that of the disordered alloy, and (ii) the ordered structure is characterized by an “ordering vector” corresponding to a special  $k$  point of the parent disordered fcc lattice. In this paper we have used structures from the [001] ordering vector family: the  $L1_0$  (or CuAu-I) structure for the ordered  $AB$  compound and the  $L1_1$  ( $\text{Cu}_3\text{Au}$ ) structure for  $A_3B$  and  $AB_3$ . [More general choices are possible within the context of bulk phase diagrams, as discussed in Ref. 60(a).] These structures are those observed<sup>60(c),60(d)</sup> in the phase diagram of  $\text{Cu}_{1-x}\text{Au}_x$ ; the parameters  $\{\Delta H, C_{11}, C_{12}\}$  for  $\text{Cu}_{4-n}\text{Au}_n$  ordered compounds were taken from measured low-temperature experimental data (including alloy-induced modifications of cluster properties<sup>67</sup>) as described in detail in Ref. 60(c). In bulk cluster-variation calculations within the tetrahedron approximation these values (given in Table I) reproduce quite well [Figs. 3 and 7(a) below] the measured bulk phase diagram.

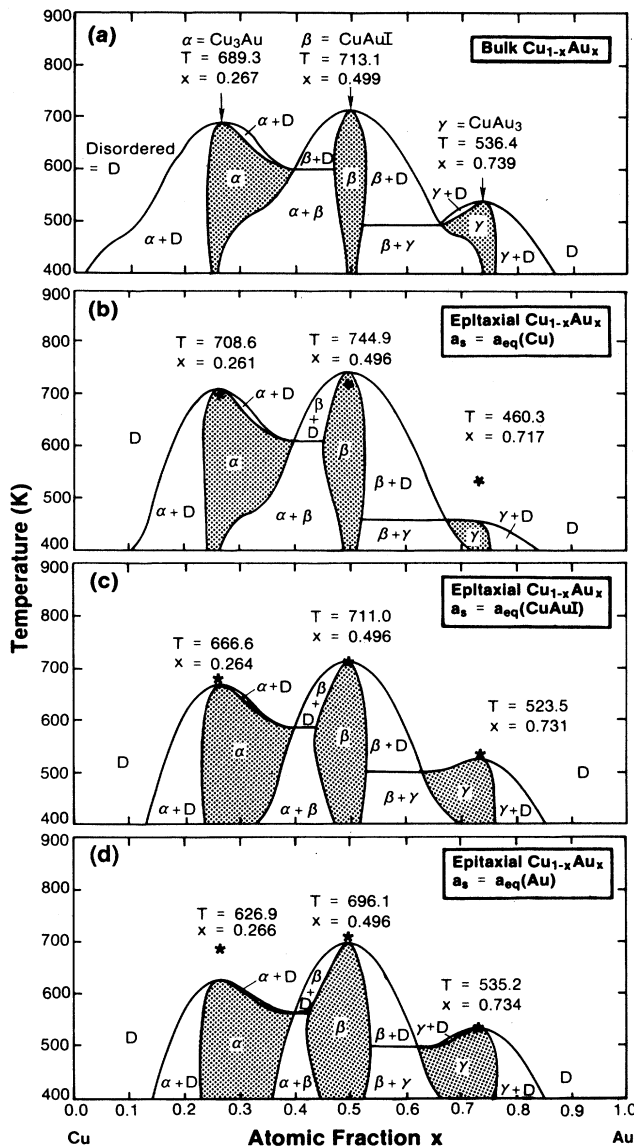


FIG. 7. Phase diagrams for  $\text{Cu}_{1-x}\text{Au}_x$  in bulk, (a), and epitaxially for [001] substrates with  $a_s = a_{\text{eq}}[\text{Cu}]$ ,  $a_{\text{eq}}[\text{CuAu-I}]$ , and  $a_{\text{eq}}[\text{Au}]$ , (b), (c), and (d), respectively. Shaded areas indicate single-phase ordered compounds; asterisks in (b)–(d) indicate bulk order-disorder transition temperatures.

## 2. $\text{GaAs}_x\text{Sb}_{1-x}$

The cluster description described above also applies to the ternary clusters  $A_{4-n}B_nC$  relevant to pseudobinary  $A_{1-x}B_xC$  alloys. These clusters may be taken from ternary Landau-Lifshitz  $A_{4-n}B_nC_4$  structures analogous to those for binary compounds above: a CuAu-I-like  $ABC_2$  structure<sup>7(a)</sup> and the “luzonite” structure<sup>7(a)</sup> for  $A_3BC_4$  and  $AB_3C_4$ . Each ternary structure has, in addition to the unit-cell lattice parameter  $a$  and a tetragonal dimension  $c$ , cell-internal structural parameters describing the positions of the atoms of the common  $C$  sublattice; see

Refs. 7(a), 8(b), and 60(a) for pictures of the unit cells and the structural parameters. These parameters must be relaxed for each value of the external constraint (in bulk for fixed cell volume, and epitaxially for fixed  $a_{\parallel} = a_s$ ). For convenience we characterize these  $A_{4-n}B_nC_4$  compounds by cubic elastic constants, although they are strictly speaking tetragonal.<sup>68</sup>

The parameters  $\{\Delta H_n\}$  were determined<sup>68</sup> in two different ways, which illustrate the crucial role played by the purely cluster property  $\Delta H_n$ , absent entirely from phenomenological descriptions:

**Model I:  $\Delta H_n$  from valence force field.** First-principles calculations of the total energy, using the full-potential linear augmented-plane-wave (LAPW) method,<sup>69</sup> were performed<sup>41</sup> for the pure constituents GaAs and GaSb in the zinc-blende structure as a function of the lattice parameter  $a$  (for bulk), and for fixed  $a_s$  as a function of  $c$  (under epitaxial conditions). Least-squares fits were then made to the data, including anharmonic (third-order elastic constant) contributions to the conventional cubic harmonic elastic constants, to extract  $C_{11}$  and  $C_{12}$  for each pure material. From these bond-bending and bond-stretching force constants were determined for Ga—As and Ga—Sb bonds, which were then used in the valence-force-field (VFF) method<sup>70</sup> to find VFF formation enthalpies  $\Delta H_n$  of the ordered  $\text{Ga}_4\text{As}_n\text{Sb}_{4-n}$  compounds. The  $a_{\text{eq}}$  and bulk modulus  $(C_{11} + 2C_{12})/3$  of  $\text{Ga}_4\text{As}_n\text{Sb}_{4-n}$  ordered compounds for  $n = 1, 2, 3$  were also calculated from first principles, and  $C_{11}$  and  $C_{12}$  for each were found using an assumed linear variation of  $C_{12}/C_{11}$  with  $n$ . Results are given in Table II; the nearest-neighbor tetrahedron cluster variation method (CVM) approximation [Fig. 8(a) below] then predicts a bulk miscibility gap of 1245 K, in reasonable agreement with the extrapolated experimental value<sup>71</sup> of about 1100 K. This VFF approximation is expected to represent well harmonic elastic response, but tends to underestimate bulk formation enthalpies for isovalent intersemiconductor compounds  $A_nB_{4-n}C_4$ . This is primarily due to the omission in VFF of repulsive chemical interactions in the ternary.<sup>72</sup>

**Model II:  $\Delta H_n$  from first principles.** We also show in Table II formation enthalpies calculated directly from first principles (model II). Using these values and elastic constants found from VFF calculations, the tetrahedron CVM predicts a bulk miscibility-gap temperature of 1633 K [Fig. 9(a) below].

It is useful to contrast within models I and II the terms  $\Delta H_{\text{bk}} + \Delta E_{\text{ES}} = \delta H_{\text{ep}}$  [Eq. (2.9)] determining epitaxial stability. A strictly strain property such as  $\Delta E_{\text{ES}}$  [Eq. (2.10)] is generally well represented by VFF (although anharmonic errors may occasionally result in incorrect trends with  $a_s$ ). For ordered CuAu-I  $\text{Ga}_2\text{AsSb}$  on a lattice-matched substrate, for example, both VFF and LAPW predict  $\Delta E_{\text{ES}} = -0.929$  kcal/mol. However, differences between VFF and LAPW values of the  $\Delta H_n$  lead to very different expectations for the epitaxial phase diagrams. VFF predicts  $\Delta H_{\text{bk}} = 0.87$  kcal/mol, an epitaxial formation enthalpy  $\delta H_{\text{ep}}(a_s) = -0.929 + 0.87 = -0.059$  kcal/mol, and so epitaxial ordering, while

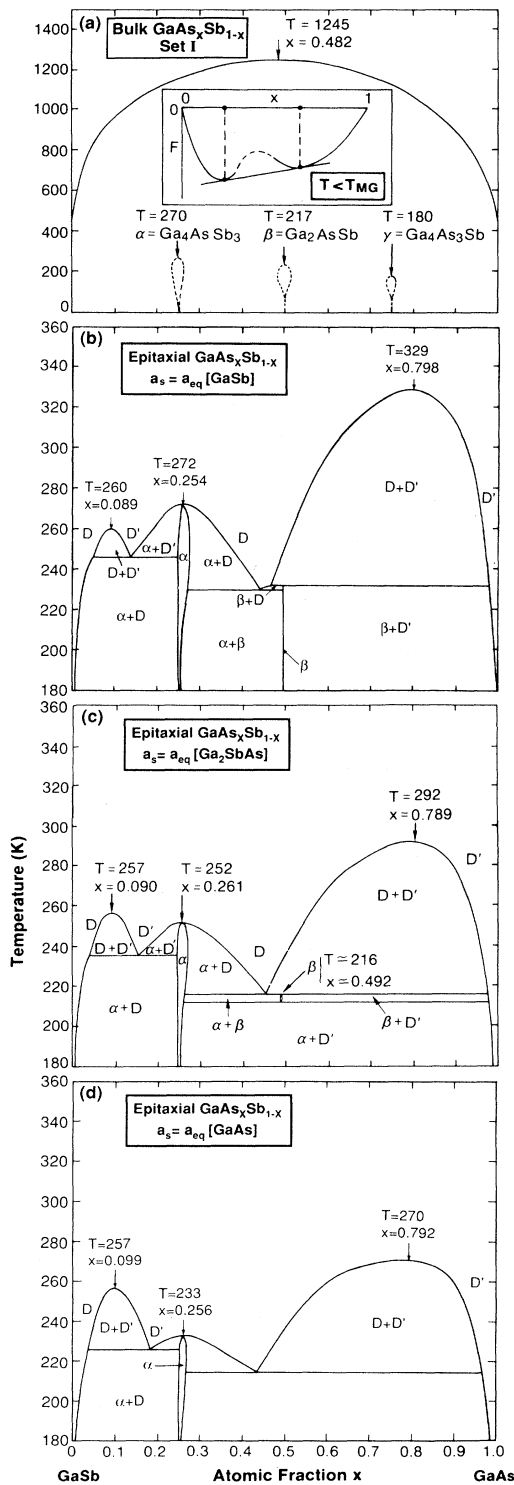


FIG. 8. Phase diagrams for  $\text{GaAs}_x\text{Sb}_{1-x}$  using model I data, in bulk (a) and epitaxially on [001]-oriented substrate with  $a_s = a_{\text{eq}}[\text{GaSb}]$ ,  $a_{\text{eq}}[\text{Ga}_2\text{AsSb}]$ , and  $a_{\text{eq}}[\text{GaAs}]$ , (b)–(d), respectively. In (a) dashed lines indicate spinodals of metastable ordered compounds; inset shows schematic  $x$  dependence of free energy.  $\alpha = \text{Ga}_4\text{AsSb}_3$ ,  $\beta = \text{Ga}_2\text{AsSb}$ ,  $\gamma = \text{Ga}_4\text{As}_3\text{Sb}$ ;  $D + D'$  indicates miscibility gap.

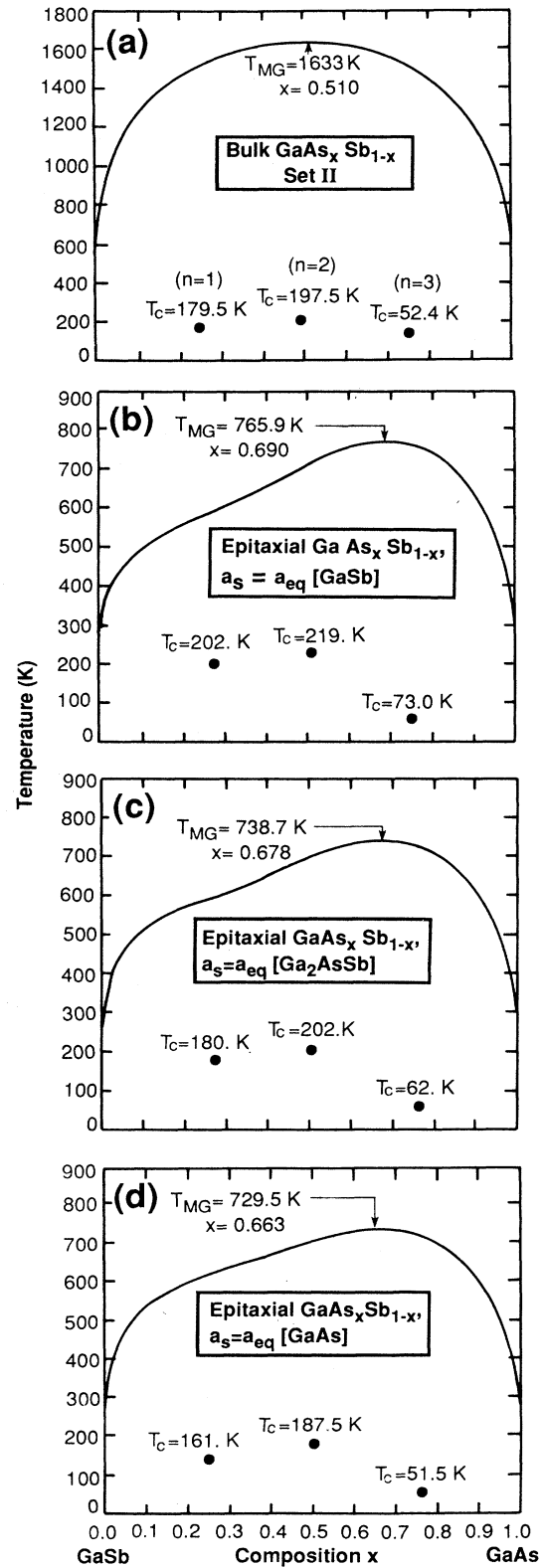


FIG. 9. Phase diagrams for  $\text{GaAs}_x\text{Sb}_{1-x}$  as in Fig. 8, but using model II data. Solid circles indicate top of spinodals for epitaxially metastable ordered phases.

LAPW predicts  $\Delta H_{\text{bk}} = 1.33$  kcal/mol,  $\delta H_{\text{ep}} = -0.929 + 1.33 = +0.401$  kcal/mol, and thus *no ordering*. Thus models I and II for  $\text{Ga}_2\text{AsSb}$  correspond to the two generic cases shown in Fig. 2; we will therefore discuss both models in parallel below.

### B. Variational determination of cluster probabilities

Given  $A_{4-n}B_n$  cluster parameters as input, the cluster probabilities  $P_n(x, T)$  and entropy  $S$  may be simultaneously determined under bulk or epitaxial conditions by minimizing the alloy free energy  $F = E - TS$  with respect to the  $\{P_n\}$  using the cluster variation method of Kikuchi.<sup>67,73</sup> In this study we work within the tetrahedron approximation (i.e., the largest configurational figure retained is the tetrahedron, as discussed in Sec. III B), so that  $n$  runs over the values 0 (pure  $A$  clusters) to 4 (pure  $B$  clusters). In a pseudobinary  $A_{1-x}B_xC$  alloy some tetrahedra contain a  $C$  atom and some do not, but only the configurational degrees of freedom of the mixed  $A$ - $B$  sublattices are relevant, so that the same CVM approximation may be consistently applied to both  $\text{Cu}_{1-x}\text{Au}_x$  and  $\text{GaAs}_x\text{Sb}_{1-x}$  alloys.

The tetrahedron approximation includes nearest-neighbor interactions through four-body terms. It therefore cannot distinguish among structures differing beyond nearest neighbors, e.g., at  $x = 0.5$ , ordering into the  $\text{CuAu}$ -I-like  $ABC_2$  structure from ordering into the  $A_2B_2C_4$  chalcopyrite structure, or, at  $x = 0.25$  or  $0.75$ , luzonite from famatinitelike ordering. We also do not include the  $\text{CuPt}$  structure commonly observed experimentally for  $ABC_2$ . Inclusion of multiatom interactions with distant neighbors (up to fourth) determined by LAPW calculations within the CVM framework can distinguish among such competing ordered phases and produces very good agreement with the experimental phase diagram<sup>60(a)</sup> with no adjustable parameters: e.g., a predicted maximum miscibility gap temperature of  $\sim 1100$  K, close to the experimental extrapolated value. Such extensive calculations (using from eight to ten equations of state) are beyond the scope of the present work, so we retain the tetrahedron approximation and use five cluster equations of state for both  $\text{Cu}_{1-x}\text{Au}_x$  and  $\text{GaAs}_x\text{Sb}_{1-x}$ .

Ordered  $A_{4-n}B_n$  compounds may exist for compositions away from the nominal stoichiometric compositions  $x_n = n/4$  and for finite temperatures, where they acquire finite entropy. We emphasize that we also use the mixture of clusters description for *ordered* compounds; as  $T \rightarrow 0$  for ordered phase  $m$ ,  $P_n(x, T) \rightarrow \delta_{n,m} \delta(x - x_n)$ , where  $\delta_{n,m}$  is the Kronecker delta function and  $\delta(x - x_n)$  is the Dirac delta function. The ordered character of such a phase is reflected by symmetries of the sublattice occupations in the CVM description. For example, the  $A_3B$  phase corresponds to periodic repetition of an oriented  $A_3B$  tetrahedron, with three equivalent and one inequivalent sublattices, while for a disordered alloy all sublattices are equivalent by symmetry. Above order-disorder temperatures CVM solutions of the required symmetry degenerate into those of the (higher-symmetry) disordered phase.

### C. Validity of the harmonic approximation

A cluster description of, e.g., a bulk  $A_{1-x}B_x$  alloy requires cluster energy functions  $\Delta E_{\text{bk}}^{(n)}(a)$  for the range (at zero pressure)  $a_{\text{eq}}[A] \leq a_{\text{eq}}(x, T) \leq a_{\text{eq}}[B]$ , corresponding to the full composition range. Since  $\Delta a = a_{\text{eq}}[B] - a_{\text{eq}}[A]$  may be large, the  $\Delta E_{\text{bk}}^{(n)}(a)$  may be expected to be significantly anharmonic over this range. In previously reported bulk alloy calculations,<sup>60</sup> this fact was reflected in the choice of the anharmonic Murnaghan equation of state for  $\Delta E_{\text{bk}}^{(n)}$ . This form, known to describe adequately real materials, is

$$\Delta E_{\text{bk}}(V) = \Delta H + BV_{\text{eq}}/(1-B') + BV/B' - [BV_{\text{eq}}/B'(1-B')](V/V_{\text{eq}})^{1-B'}, \quad (4.1)$$

where  $V_{\text{eq}}$  is the equilibrium volume,  $B$  is the bulk modulus at pressure  $P = 0$ , and  $B' = (dB/dP)_{P=0}$ . In this paper we consistently use (a) a harmonic approximation, corresponding to the choice  $B' = -1$  in Eq. (4.1); and (b) a lattice-parameter  $a$  (not  $V$ ) representation corresponding, if  $V \propto a^3$ , to neglect of terms of order  $(a - a_{\text{eq}})^3$  (as required in a harmonic  $a$  representation). In Fig. 3 we contrast the phase diagram for  $\text{Cu}_{1-x}\text{Au}_x$  using the harmonic (solid line) and Murnaghan (dashed lines) forms [see Ref. 60(c)]. Apart from the absence of an apparent triple point around  $x = 0.65$  in the anharmonic case, there are no significant differences over the full temperature and composition range. One reason for this is that at compositions where alloy clusters are strained enough for anharmonic effects to become important, their total energies  $\Delta E_{\text{bk}}^{(n)}[a(x)]$  are also large, so their relative probabilities  $P_n(x)$  are suppressed when minimizing the free energy for each phase using the cluster variation method. Errors associated with anharmonicity are probably smaller than those implicit in the nearest-neighbor tetrahedron approximation CVM described above, and for purposes of comparing bulk and epitaxial phase diagrams, a strictly harmonic description is adequate.

## V. MACROSCOPIC AND MICROSCOPIC PROPERTIES OF EPITAXIAL VERSUS BULK ALLOYS

In examining calculated properties of epitaxial alloys, it is useful to remember that our treatment is valid provided (i) the epitaxial film thickness  $h$  is thin enough that the film remains coherent (Sec. II A), and (ii)  $h$  exceeds a few monolayers, so surface free energies are negligible (Sec. III D). Point (i) restricts the validity of our results to a "window" in  $x$  in the  $(x, T)$  phase diagram centered on the value where the alloy is lattice matched to a given substrate. The width of this window may be estimated using the Appendix. For simplicity we will ignore this restriction below.

### A. Excess enthalpies and ordering in bulk and epitaxial alloys

The essential physics of epitaxy may be understood by contrasting actual calculated formation enthalpies  $\Delta H$  for bulk and epitaxial conditions. Figure 4 shows

TABLE III. Bulk ( $\Delta H_{\text{bk}}$ ) and epitaxial ( $\delta H_{\text{ep}}$ ) excess enthalpies and disordering energies  $\Delta E_{\text{dis}}$  (kcal per mol fcc sites) for  $\text{Cu}_{4-n}\text{Au}_n$  ordered compounds at ( $T=0$ ) and disordered  $\text{Cu}_{1-x}\text{Au}_x$  alloy (at  $T=800$  K) for [001] substrates;  $\Delta E_{\text{dis}}$  is their difference.

	$\Delta H_{\text{bk}}$	$\delta H_{\text{ep}}$	
		$a_s = a_{\text{eq}}[\text{Cu}]$	$a_s = a_{\text{eq}}[\text{CuAu-I}]$
$\text{Cu}_3\text{Au}$	-1.556	-1.934	-2.175
$\text{Cu}_{0.75}\text{Au}_{0.25}$	-0.988	-1.356	-1.617
$\Delta E_{\text{dis}}$	0.568	0.578	0.558
$\text{CuAuI}$	-2.100	-2.467	-2.832
$\text{Cu}_{0.5}\text{Au}_{0.5}$	-1.392	-1.738	-2.124
$\Delta E_{\text{dis}}$	0.708	0.729	0.708
$\text{CuAu}_3$	-1.373	-1.393	-1.815
$\text{Cu}_{0.25}\text{Au}_{0.75}$	-0.886	-0.958	-1.336
$\Delta E_{\text{dis}}$	0.487	0.435	0.479

$\Delta H^D(x)$  for the disordered ( $D$ ) alloy (at  $T=800$  K) and  $\Delta H_n^O$  for ordered ( $O$ ) compounds  $n$  (at  $T=0$ ) for a typical "ordering" alloy,  $\text{Cu}_{1-x}\text{Au}_x$  under bulk conditions and epitaxially for (001) substrates lattice matched to  $x=0$ ,  $x \approx 0.5$ , and  $x=1$ . For such bulk ordering alloys we note that  $\Delta H^D \leq 0$ ,  $d^2\Delta H^D/dx^2 > 0$ , and  $\Delta H_n^O < 0$ . Figures 5 and 6 show analogous results for  $\text{GaAs}_x\text{Sb}_{1-x}$ , a typical "phase-separating" alloy, with  $\Delta H^D \geq 0$ ,  $d^2\Delta H^D/dx^2 < 0$ , and  $\Delta H_n^O > 0$ , using the input parameters shown in Table II for the two cases  $\delta H_{\text{ep}} < 0$  [model I, Fig. 5, corresponding to the situation shown schematically in Fig. 2(a)] and  $\delta H_{\text{ep}} > 0$  [model II, Fig. 6, corresponding to Fig. 2(b)]. We note the following.

(i) At the lattice-matched composition, the bulk (solid lines) and epitaxial (dashed lines)  $\Delta H$  coincide, since epitaxy poses no constraint [Eq. (3.14)].

(ii) Away from the lattice-matched composition for a given substrate, the constraint  $a_{\parallel} = a_s$  raises the energy of epitaxial ordered compounds (open circles or solid triangles) and the disordered epitaxial alloy by *different amounts*; thus, order-disorder transition temperatures change under epitaxial conditions.

(iii) The epitaxial constraint makes a positive contribu-

tion to the *curvature* of  $\Delta H^D$  with respect to composition. For phase-separating alloys a "miscibility gap" is associated (Sec. VB 2) with regions where  $d^2\Delta F/dx^2 = d^2\Delta H/dx^2 - T d^2\Delta S/dx^2 < 0$ . Since (Sec. VD)  $-T d^2\Delta S/dx^2 > 0$  and we will find that the mixing entropy  $\Delta S$  is virtually unmodified by the epitaxial constraint, the less negative curvature of the epitaxial  $\Delta H(x)$  implies miscibility gap temperatures will be lower under epitaxial conditions than in bulk. Figures 4-6 [or Eq. (3.14)] show that this is so *even on a lattice-matched substrate*. Ordering alloys do not exhibit a miscibility gap since  $d^2\Delta H/dx^2 > 0$ .

(iv) The epitaxial formation enthalpies  $\delta H_{\text{ep}}^{(n)}$  (Tables III and IV) may be used to determine whether or not a given ordered phase will occur as a stable phase in the epitaxial phase diagram.

(a) For  $\text{Cu}_{1-x}\text{Au}_x$  (Fig. 4) the  $\Delta H_n$  ( $< 0$ ) for all ordered epitaxial compounds lie *below* the energy of the epitaxially constrained constituents (i.e.,  $\delta H_{\text{ep}} < 0$ ; see Table III). We thus expect all these phases to remain in the epitaxial phase diagrams for all three substrates, with only quantitative distortions of the bulk phase diagram due to the epitaxial constraint.

TABLE IV. Bulk ( $\Delta H_{\text{bk}}$ ) and epitaxial ( $\delta H_{\text{ep}}$ ) excess enthalpies and disordering energies  $\Delta E_{\text{dis}}$  (kcal/mol fcc-site) for ordered  $\text{Ga}_4\text{As}_n\text{Sb}_{4-n}$  ordered compounds ( $T=0$ ) and disordered  $\text{GaAs}_x\text{Sb}_{1-x}$  alloy at  $T=1400$  K for model I (VFF) and 1700 K for model II (LAPW) for [001] substrates.  $\Delta E_{\text{dis}}$  is their difference. Note that model I gives  $\delta H_{\text{ep}} < 0$  for some structures while  $\delta H_{\text{ep}} > 0$  for model II.

	$\Delta H_{\text{bk}}$		$\delta H_{\text{ep}}$		$\delta H_{\text{ep}}$		$\delta H_{\text{ep}}$	
	I	II	$(a_s = a_{\text{eq}}[\text{GaSb}])$		$(a_s = a_{\text{eq}}[\text{Ga}_2\text{AsSb}])$		$(a_s = a_{\text{eq}}[\text{GaAs}])$	
			I	II	I	II	I	II
$\text{Ga}_4\text{AsSb}_3$	0.619	1.01	-0.126	0.265	-0.091	0.300	-0.051	0.340
$\text{GaAs}_{0.25}\text{Sb}_{0.75}$	0.954	1.268	0.220	0.535	0.234	0.546	0.254	0.564
$\Delta E_{\text{dis}}$	0.335	0.258	0.346	0.270	0.325	0.246	0.305	0.224
$\text{Ga}_2\text{AsSb}$	0.870	1.33	-0.085	0.375	-0.057	0.403	-0.019	0.441
$\text{GaAs}_{0.5}\text{Sb}_{0.5}$	1.240	1.668	0.308	0.739	0.313	0.741	0.331	0.756
$\Delta E_{\text{dis}}$	0.370	0.338	0.393	0.364	0.370	0.338	0.350	0.315
$\text{Ga}_4\text{As}_3\text{Sb}$	0.681	1.15	0.005	0.474	0.009	0.478	0.026	0.495
$\text{GaAs}_{0.75}\text{Sb}_{0.25}$	0.928	1.267	0.272	0.613	0.263	0.603	0.267	0.604
$\Delta E_{\text{dis}}$	0.247	0.117	0.267	0.139	0.254	0.125	0.241	0.109

(b) The situation is very different for  $\text{GaAs}_x\text{Sb}_{1-x}$  (Table IV). Here  $\Delta H^D(x_n) > \Delta H_n > 0$  at  $x_n = \frac{1}{4}, \frac{1}{2}, \frac{3}{4}$  (Table II and Figs. 5 and 6), so the bulk phase diagram shows no stable ordering, although this inequality implies metastable ordering is possible.<sup>74</sup> Since  $\delta H_{\text{ep}} = \Delta H_{\text{bk}} + \Delta E_{\text{ES}}$  may become negative, however, epitaxial ordering may occur even when none is present in bulk. As in Fig. 2, we can distinguish the two cases, *epitaxial stabilization of an ordered compound*,  $\delta H_{\text{ep}} < 0$ , the case for model I in Table II for  $\text{Ga}_4\text{As}_3\text{Sb}$  and  $\text{Ga}_2\text{AsSb}$  on all three substrates (Table IV); or *epitaxial ordered compounds remain unstable*,  $\delta H_{\text{ep}} > 0$ , the case (Table IV) for model II of Table II, or for  $\text{Ga}_4\text{As}_3\text{Sb}$  for all three substrates for model I. We next examine how well these simple expectations explain calculated phase diagrams.

## B. Epitaxial versus bulk phase diagrams

### 1. Ordering alloys: $\text{Cu}_{1-x}\text{Au}_x$

We turn first to the  $\text{Cu}_{1-x}\text{Au}_x$  alloy, typical of ordering systems, whose bulk phase diagram is well characterized experimentally.<sup>60(c)-60(f)</sup> In Fig. 7(a) we show the bulk phase diagram, calculated as described in Sec. IV A 1; order-disorder critical temperatures agree well with experiment [see Refs. 60(c) and 60(d) and references therein]. Figures 7(b)–7(d) show the corresponding epitaxial phase diagram for the three different substrates whose excess enthalpies are shown in Fig. 4.

Contrasting bulk and epitaxial phase diagrams we note (i) epitaxial expansion of the region (especially at low temperatures) over which single phases—ordered compounds (shaded regions  $\alpha, \beta, \gamma$ ) and the disordered alloy ( $D$ )—are stable. At 400 K for  $a_s \simeq a_{\text{eq}}(0.5)$ , for example, the Cu-rich disordered alloy is epitaxially stable to  $x \simeq 0.13$ , but to only about  $x = 0.02$  in bulk. There are also (ii) corresponding reductions of two-phase coexistence ( $\alpha + D, \gamma + D, \alpha + \beta, \beta + \gamma$ ). In increasing  $a_s$  from  $a_{\text{eq}}[\text{Cu}]$  to  $a_{\text{eq}}[\text{Au}]$  there is (iii) a systematic expansion of the region of stability of the order compounds and (iv)  $\sim 80$  K excursions in order-disorder temperatures. All four effects will be discussed in Sec. V C.

Table III shows that the relative energy  $\Delta E_{\text{dis}}(x_n) = \Delta H^D(x_n) - \Delta H_n^O$  of an ordered phase and a disordered alloy of the same composition differ under bulk and epitaxial conditions. For the  $\text{Cu}_3\text{Au} \rightarrow \text{Cu}_{0.75}\text{Au}_{0.25}$  disordering reaction, for example  $\Delta E_{\text{dis}}$  is 0.568 kcal/mol in bulk, but only 0.537 kcal/mol on an Au substrate. Since we expect an order-disorder transition temperature proportional to  $\Delta E_{\text{dis}}$ , the transition temperature on this substrate will be lower than in bulk; these and other epitaxy-induced distortions of the phase diagram are discussed in Sec. V C. However, even on substrates lattice matched to the bulk compounds, order-disorder temperatures differ slightly under bulk [Fig. 7(a)] and epitaxial conditions, reflecting the different elastic properties of the ordered and disordered alloys. While in bulk both phases are free to relax to their respective  $a_{\text{eq}}$ , on a fixed substrate, e.g., that of ordered CuAu-I in Fig. 7(c), only one can be strain free, so there is a slight shift in  $T_c$  with respect to bulk. Such subtleties are clearly

beyond a continuum elastic description of an alloy and require a cluster-based approach.

### 2. Phase-separating alloys

In Figs. 8 and 9 we show phase diagrams for  $\text{GaAs}_x\text{Sb}_{1-x}$ , a typical “phase-separating” system, using the parameters of data sets I and II (Table II), respectively. The principal features of the *bulk* phase diagram in either case [Figs. 8(a) and 9(a)] are (i) a miscibility gap separating the disordered phase above  $T_{\text{MG}}$  (experimental extrapolated value:<sup>71</sup>  $\sim 1100$  K) from a GaSb- and GaAs-rich two-phase mixture below, and (ii) metastable  $\text{Ga}_4\text{As}_m\text{Sb}_{4-m}$  ordered compounds [indicated by dashed spinodals  $d^2F/dx^2 = 0$  defining the limits of stability in Fig. 8(a) and by solid dots in Fig. 9(a) showing the maximum of the spinodal]. A miscibility gap corresponds to coexistence between disordered phases of two different compositions, with a homogeneous alloy of intermediate alloy compositions not attainable. This situation reflects the double-hump structure shown schematically in the inset to Fig. 8(a). The maximum metastable ordering temperatures and miscibility temperatures are different for sets I and II, reflecting the more positive  $\Delta H_n$  in the latter.

The epitaxial phase diagrams [Figs. 8(b)–8(d) and 9(b)–9(d)] for the three substrates in Figs. 5 and 6 differ profoundly from their bulk counterparts.

(i) The miscibility gap is strongly suppressed, by an amount  $\Delta T_{\text{MG}}(x)$  as large as  $\sim 975^\circ\text{C}$  using model I ( $\sim 900^\circ\text{C}$  in model II), and becomes significantly asymmetric under epitaxial conditions. Despite a  $\sim 31\%$  difference in bulk miscibility temperatures (which contain important contributions from the  $\Delta H_n$ ) between models I and II, there is only a  $\sim 6\%$  difference in  $\Delta T_{\text{MG}}$ . Equations (3.11), (3.14), and (3.15) show that the alloy epitaxial strain energy  $E_{\text{ES}}(a_s, x, T)$  depends only weakly on the  $\Delta H_n$  (via the cluster probabilities). Like other quantities which do not depend explicitly on the  $\Delta H_n$ ,  $\Delta T_{\text{MG}}(x)$  can be reasonably estimated by continuum elastic descriptions (see Sec. VI C 3), while the asymmetry about  $x = 0.5$  is a manifestation of the asymmetry of the  $\Delta H_n$ . Surprisingly,  $\Delta T_{\text{MG}}(a_s, x)$  depends only very weakly on the substrate lattice parameter  $a_s$ . As noted in the Introduction, bulk-insoluble alloys have recently been grown epitaxially over a large composition range, e.g.,  $\text{GaAs}_x\text{Sb}_{1-x}$  (Ref. 16) and  $\text{GaP}_x\text{Sb}_{1-x}$  (grown<sup>15</sup>  $\sim 1200$  K below the bulk miscibility gap).

(ii) The obvious difference between models I and II is that at low temperatures for the three substrates examined, I predicts stable ( $\delta H_{\text{ep}} < 0$ )  $\text{Ga}_4\text{As}_n\text{Sb}_{4-n}$  epitaxial compounds for  $n = 1, 2$ , while II does not ( $\delta H_{\text{ep}} > 0$ ), as shown in Table IV. The calculated phase diagrams show no epitaxially stable ordered compounds for model II (Fig. 9), while model I (Fig. 8) exhibits both ordered phases and miscibility gaps in the epitaxial case. First-principles calculations<sup>41</sup> suggest, however, that, e.g., at  $x = \frac{1}{2}$ , ordering into a chalcopyrite structure is more likely than the CuAu-I-like structure whose  $\Delta H$  was used in these calculations (and at  $x = \frac{1}{4}$  or  $\frac{3}{4}$ , ordering into a famatinite, rather than luzonite, phase is preferred).

Moreover, as discussed in Sec. III D, the CuPt ordering most frequently observed<sup>2</sup> is probably catalyzed by surface effects not explained by our approach. Interestingly, ordering<sup>5</sup> of  $\text{In}_{1-x}\text{Ga}_x\text{As}$  grown by the near-equilibrium LPE method near  $x=0.48$  appears famatinitelike, in qualitative agreement with the relatively large region of stability of  $\text{Ga}_4\text{AsSb}_3$  in Fig. 8. The presence or absence of a given ordered phase in the phase diagram may also be modified by finite temperature effects: although expected to exist for all substrates on the basis of the  $T=0$  epitaxial model I  $\delta H_{\text{ep}}$ , Fig. 8 shows CuAu-I-like  $\text{Ga}_2\text{AsSb}$  to be stable to  $T=0$  for  $a_s = a_{\text{eq}}[\text{GaSb}]$ , entropy stabilized for a narrow temperature range for  $a_s = a_{\text{eq}}[\text{Ga}_2\text{AsSb}]$ , and absent for  $a_s = a_{\text{eq}}[\text{GaAs}]$ . Thus the  $T=0$  epitaxial formation enthalpies are only a guide to which phases may be present.

### C. Modeling epitaxial distortions of phase diagrams

Thus far bulk and epitaxial  $A_{1-x}B_x$  alloys have been described as a mixture of distorted clusters. Even when such clusters are undistorted their energies  $\Delta H_n$  include<sup>60(e),60(f)</sup> an "elastic" contribution (associated with compressing  $A$  and  $B$  to  $a_n = a_{\text{eq}}[A_{4-n}B_n]$ ) and a "chemical" contribution (due to  $A$ - $B$  interactions for fixed  $a = a_n$ ). Ferreira *et al.*<sup>60(e),60(f)</sup> have shown how these may be rigorously separated if equilibrium volumes (or  $a_{\text{eq}}$ ) and elastic properties for ordered and disordered phases at a given composition  $x$  are the same. In this " $\epsilon$ - $G$ " approach, Eq. (3.7) for a bulk (bk) alloy is replaced by

$$\Delta H_{\text{bk}}(x, T) = \sum_n P_n(x, T) \epsilon_{\text{bk}}^{(n)} + G_{\text{bk}}(x), \quad (5.1)$$

where

$$G(x) = (1-x) \int_0^x y Z(y) dy + x \int_x^1 (1-y) Z(y) dy \quad (5.2)$$

with

$$Z_{\text{bk}}(x) = \frac{2}{3} a(x) B(x) (da/dx)^2. \quad (5.3)$$

The utility of this approach is that one can calculate  $G(x)$  via integration given knowledge of only elastic and structural properties [Eq. (5.3)]; in practice  $a(x)$  and  $B(x)$  are found by interpolation on the values for  $A_{4-n}B_n$  ordered compounds for  $n=0-4$ . The "chemical" or "spin-flip" energies  $\epsilon^{(n)}$  ( $n=1,2,3$ ) are then found from the  $T=0$  formation enthalpy  $\Delta H_n$  of ordered  $A_{4-n}B_n$  [for which  $P_n(x, T) = \delta_{n,m}$  in Eq. (5.1)], i.e.,

$$\epsilon_{\text{bk}}^{(n)} = \Delta H_n - G_{\text{bk}}(x_n). \quad (5.4)$$

Order-disorder transition temperatures at fixed  $x$  depend only on the  $\{\epsilon^{(n)}\}$ , since by assumption  $G(x)$  is common to both ordered and disordered phases; the  $\epsilon$ - $G$  formalism thus permits a simple analysis of strain effects on such transformations. Within the five-cluster tetrahedron  $\epsilon$ - $G$  description the transition temperatures (in K) at  $x_n = n/4$  ( $n=1,2,3$ ) are given approximately by

$$\begin{pmatrix} T^{(1)} \\ T^{(2)} \\ T^{(3)} \end{pmatrix} = \begin{pmatrix} -453.32 & 208.92 & 11.80 \\ 201.34 & -421.11 & 201.34 \\ 11.80 & 208.92 & -453.32 \end{pmatrix} \begin{pmatrix} \epsilon^{(1)} \\ \epsilon^{(2)} \\ \epsilon^{(3)} \end{pmatrix}, \quad (5.5)$$

with  $\epsilon^{(n)}$  in kcal per fcc site mol. Similar matrix relationships connect<sup>60(e)</sup> the  $\epsilon^{(n)}$  to the compositions at the ordering temperatures, latent heats of ordering, and enhancements of cluster probabilities with respect to their random values (Sec. V E below).

To understand the distortions of phase diagrams due to coherent *epitaxy* (Figs. 7-9), we may generalize the bulk  $\epsilon$ - $G$  approach above. By analogy with Eq. (5.4) for bulk,

$$\epsilon_{\text{ep}}^{(n)} = \delta H_{\text{ep}}^{(n)} - G_{\text{ep}}(a_s, x_n) = \Delta H_n - \tilde{G}_{\text{ep}}(a_s, x_n), \quad (5.6)$$

where [see Eq. (2.9)]

$$\tilde{G}_{\text{ep}}(a_s, x) = G_{\text{ep}}(a_s, x) - \Delta E_{\text{ES}}(a_s, x) \quad (5.7)$$

with

$$\begin{aligned} \Delta E_{\text{ES}}(a_s, x) = & \frac{9}{8} \{ a(x)q(x)B(x)[a_s - a(x)]^2 \\ & - (1-x)a(0)q(0)B(0)[a_s - a(0)]^2 \\ & - xa(1)q(1)B(1)[a_s - a(1)]^2 \}. \end{aligned} \quad (5.8)$$

Similarly, Eq. (5.3) is replaced by

$$Z_{\text{ep}}(a_s, x) = \frac{1}{4} a(x) A(x) [dc(a_s, x)/dx]^2, \quad (5.9)$$

[and  $G_{\text{ep}}$  is given by Eq. (5.2) with  $Z = Z_{\text{ep}}$ ] where  $c(a_s, x)$  and  $A(x)$  depend on orientation [Eqs. (2.3) and (2.4)]. For fixed substrate  $q(x)$ ,  $A(x)$ ,  $B(x)$ , and  $a(x)$  (hence  $\tilde{G}_{\text{ep}}$ ) depend only on composition; in practice they are found by interpolation on the values for  $A_{4-n}B_n$  for  $n=0-4$ .

Given the same cluster ingredients described in Secs. V A and V B, the  $\epsilon$ - $G$  analysis permits predictions of the order-disorder transition temperatures without performing CVM calculations. In Table V we give values of the "spin-flip" energies  $\epsilon^{(n)}$  and order-disorder transition temperatures, for bulk and epitaxial [ $a_s = a_{\text{eq}}(x=0.5)$ ]  $\text{Cu}_{1-x}\text{Au}_x$  and  $\text{GaAs}_x\text{Sb}_{1-x}$  (model-I) alloys. We note that (i) critical temperatures calculated within the  $\epsilon$ - $G$  approach agree quite well with those found from full CVM calculations; and (ii) for both alloy systems  $\epsilon^{(n)} < 0$ . The dominance of the diagonal matrix elements in Eq. (5.5) means that positive (stable or metastable) order-disorder transition temperatures require  $\epsilon_n < 0$ , which also enhances<sup>60(e),60(f)</sup> the probabilities of mixed  $A_{4-n}B_n$  clusters with respect to their random values (for both  $\text{Cu}_{1-x}\text{Au}_x$  and  $\text{GaAs}_x\text{Sb}_{1-x}$  as discussed in Sec. V E below).

We may also use the epitaxial  $\epsilon$ - $G$  analysis to understand the systematic distortions with  $a_s$  of the epitaxial phase diagram with respect to bulk. For bulk alloys it was found that including the elastic energy  $G_{\text{bk}}(x)$  resulted in two modifications with respect to the strain-free ( $\epsilon$ -only) phase diagram: (i) single-phase regions (e.g., ordered compounds or the homogeneous disordered alloy) narrow in composition, and (ii) regions of two-phase coexistence (e.g.,  $\alpha + D$  or  $\alpha + \beta$  in Fig. 7 for  $\text{Cu}_{1-x}\text{Au}_x$ ) expand. Under epitaxial conditions the corresponding observations are that if  $\tilde{G}_{\text{ep}}(a_s, x) > G_{\text{bk}}(x)$  single-phase regions narrow and two-phase regions expand, with respect to their bulk counterparts (the opposite is true if

TABLE V.  $\epsilon^{(n)}$  (in kcal/fcc-site mol) and order-disorder temperatures (K) found from the  $\epsilon$ - $G$  model under bulk and epitaxial [with  $a_s = a_{eq}(x = 0.5)$ ] conditions; model I results are used for  $\text{GaAs}_x\text{Sb}_{1-x}$ . Temperatures calculated within CVM are in parentheses.

	$\epsilon^{(1)}$	$\epsilon^{(2)}$	$\epsilon^{(3)}$	$T^{(1)}$	$T^{(2)}$	$T^{(3)}$
			$\text{Cu}_{1-x}\text{Au}_x$			
Bulk	-4.2073	-5.6302	-3.9365	684.5 (689.3)	731.3 (713.1)	558.6 (536.4)
Epitaxial	-4.1381	-5.5673	-3.8826	666.9 (666.6)	729.6 (711.0)	548.1 (523.5)
			$\text{GaAs}_{1-x}\text{Sb}_x$			
Bulk	-1.4569	-1.8335	-1.2925	262.1 (270)	218.5 (217)	185.7 (180)
Epitaxial	-1.4297	-1.8215	-1.2971	252.3 (252)	218.0 (218)	190.6

$\tilde{G}_{ep} < G_{bk}$ ). In Fig. 10 we show contour plots of the relevant differential strain energy

$$\Delta(a_s, x) = \tilde{G}_{ep}(a_s, x) - G_{bk}(x) \quad (5.10)$$

as a function of  $a_s$  and  $x$ , for  $\text{Cu}_{1-x}\text{Au}_x$  [Fig. 10(a)] and for  $\text{GaAs}_x\text{Sb}_{1-x}$  [Fig. 10(b)], for either models I or II, since they are elastically identical. For  $\text{Cu}_{1-x}\text{Au}_x$ ,  $\Delta$  is negative for most of the  $(a_s, x)$  region, implying (as seen in Fig. 7) that the regions of stability of the ordered compounds *expand* with respect to bulk. Similar remarks for  $\text{GaAs}_x\text{Sb}_{1-x}$  are more difficult to make because of the narrowness of ordered regions (present only for model I).

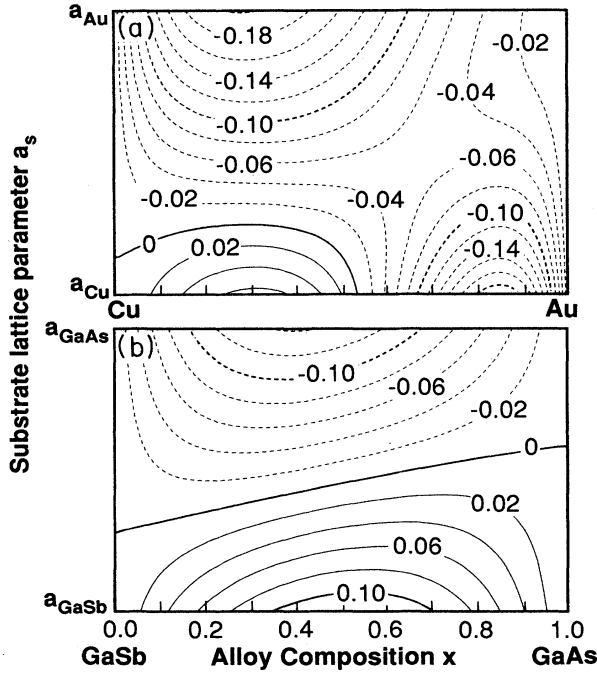


FIG. 10. Contours [kcal/(fcc site) mol] of differential strain energy [Eq. (5.10)] determining epitaxial distortions of phase boundaries and shifts in order-disorder transition temperatures, as a function of substrate lattice parameter  $a_s$  and alloy composition  $x$  for (a)  $\text{Cu}_{1-x}\text{Au}_x$  and (b)  $\text{GaAs}_x\text{Sb}_{1-x}$ .

We note that  $\Delta\epsilon^{(n)}(a_s) \equiv \epsilon_{ep}^{(n)}(a_s) - \epsilon_{bk}^{(n)} = -\Delta(a_s, x_n)$ . At the stoichiometric compositions  $x_n = 0.25, 0.5, 0.75$  the dependence of the epitaxial shifts in order-disorder transition temperatures may be found directly from Fig. 10(a), to the extent that they are dominated by the diagonal  $\Delta\epsilon^{(m)}$  in Eq. (5.5). In Fig. 11(a) we show the epitaxy-

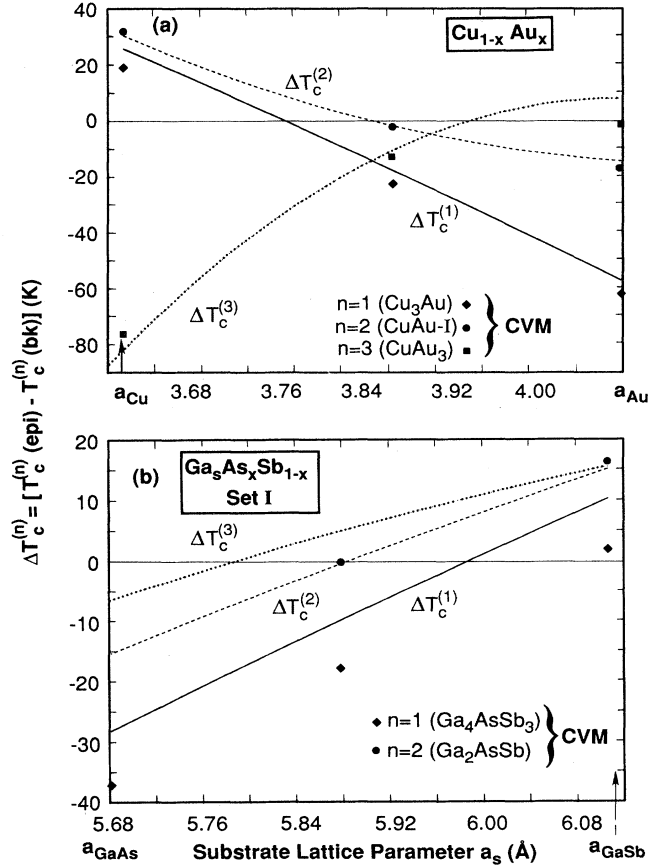


FIG. 11. Dependence on [001]-oriented substrate lattice parameter  $a_s$  of ordering temperatures for  $\text{Cu}_{1-x}\text{Au}_x$ , (a), and  $\text{GaAs}_x\text{Sb}_{1-x}$  within model I, (b). Filled symbols indicate CVM results, lines indicate results of  $\epsilon$ - $G$  theory of Sec. V C.

induced shifts of the transition temperatures (calculated within the CVM) for  $\text{Cu}_{1-x}\text{Au}_x$  as a function of  $a_s$ , together with the full  $\epsilon$ - $G$  predictions<sup>67</sup> of Eq. (5.5). The differing dependences of the  $\Delta T^{(m)}$  on  $a_s$  directly reflect the nonmonotonic behavior [for fixed  $x$  in Fig. 10(a)] of  $\Delta(a_s, x)$ . For  $\text{GaAs}_x\text{Sb}_{1-x}$  using model I the  $\Delta T^{(m)}(a_s)$  [Fig. 8(b)] are similar for all three ordered compounds (although, as noted above,  $\text{Ga}_4\text{As}_3\text{Sb}$  does not occur as a stable phase in the epitaxial phase diagrams). Using II the  $a_s$  dependence of these temperatures is similar, except that they correspond to the temperatures at which epitaxially metastable ordered compounds cease to exist.

Within the five-cluster  $\epsilon$ - $G$  description the identity  $\Delta H_{\text{ep}}[x, a_s = a_{\text{eq}}(x)] = \Delta H_{\text{bk}}(x)$  [Eq. (3.14)] is slightly violated, e.g., using random cluster probabilities [Eq. (5.11)], by  $< 1.9\%$  for  $\text{Cu}_{1-x}\text{Au}_x$  and  $< 0.3\%$  for  $\text{GaAs}_x\text{Sb}_{1-x}$  for  $0 \leq x \leq 1$ . Bulk and epitaxial order-disorder transition temperatures  $T^{(m)}$  fail to coincide on lattice-matched substrates [ $a_s = a_{\text{eq}}(x_m)$ ] by corresponding amounts:  $< 4.5^\circ\text{C}$  for  $\text{Cu}_{1-x}\text{Au}_x$  and  $< 0.8^\circ\text{C}$  for  $\text{GaAs}_x\text{Sb}_{1-x}$ . These errors are themselves much smaller than that associated with the central approximation of the  $\epsilon$ - $G$  analysis, that elastic properties are independent of the state of order.

#### D. Thermodynamic properties of epitaxial versus bulk alloys

Calculations or measurements of alloy thermodynamic properties conventionally display *excess* quantities, i.e., for the thermodynamic functions  $K = F, S, H$ , etc., one defines  $\Delta K(x) = K(A_{1-x}B_x) - (1-x)K(A) - xK(B)$ . Since  $\Delta K(x)$  is linear for  $x \rightarrow 0$  and  $x \rightarrow 1$ , the parametrization  $\Omega^K(x) \equiv \Delta K(x)/[x(1-x)]$  is often used. Within the "ideal solution," "regular solution," and "quasi-regular solution" models,  $\Omega = 0$ ,  $\Omega = \text{const}$ , and  $\Omega = \Omega(x, T)$ , respectively, where  $\Omega$  is the "interaction parameter."

Figure 12 shows such parametrizations for  $\Delta H^D(x)$  and  $\Delta S(x) \equiv S(x) - S_R(x)$ , where the ideal [random ( $R$ )] mixing entropy  $S_R(x) = -k_B[x \ln x + (1-x) \ln(1-x)]$ , under bulk and epitaxial conditions for a substrate lattice matched to the disordered alloy at  $x = 0.5$ . While deviations from  $S_R(x)$  are significant for both bulk and epitaxial  $\text{Cu}_{1-x}\text{Au}_x$  (much less so for  $\text{GaAs}_x\text{Sb}_{1-x}$  because of the higher temperature) the epitaxial constraint has virtually no effect (e.g., at 500 K,  $< 1\frac{1}{2}\%$ ) on the entropy over the entire composition range.

For the bulk alloy  $\Delta H^D(x)$  approaches zero linearly for  $x \rightarrow 0$  and  $x \rightarrow 1$ , yielding finite values of  $\Omega_{\text{bk}}^H$ . For the epitaxial alloy this is not so unless we refer epitaxial quantities to epitaxially constrained constituents (as we do in Fig. 12). The lower values of  $\Omega_{\text{ep}}^H$  (relative to  $\Omega_{\text{bk}}^H$ ) in Fig. 12 reflect the reduction in energy of the epitaxial alloy with respect to its epitaxial constituents. It is natural to parametrize  $\delta H_{\text{ep}}(x)$  in a form suggested by Eq. (3.14) and Figs. 4–6 as  $\Delta H_{\text{ep}}(x) - \Delta H_{\text{bk}}(x) = \tilde{\Omega}(x)(x - x_{\text{LM}})^2$ , where  $x_{\text{LM}}$  is the composition where the alloy is lattice matched to the substrate. For  $x_{\text{LM}} = \frac{1}{2}$  the splittings between the epitaxial and bulk curves at  $x = 0$  and 1 are given, respectively, by  $\frac{1}{4}\{d\tilde{\Omega}/dx - [\tilde{\Omega}(1) - \tilde{\Omega}(0)]\} - \tilde{\Omega}$

for  $x = 0$  and  $\frac{1}{4}\{[\tilde{\Omega}(1) - \tilde{\Omega}(0)] - d\tilde{\Omega}/dx\} - \tilde{\Omega}$  for  $x = 1$ . Since the leading terms are small, these splittings are a direct measure of  $\tilde{\Omega}(0)$  and  $\tilde{\Omega}(1)$ .

The parameter  $\Omega_{\text{bk}}^H$  for  $\text{Cu}_{1-x}\text{Au}_x$  [Fig. 12(a)] is in excellent agreement with values calculated in Ref. 60(c) (which used anharmonic cluster equations of state), and with experiment [see the discussion in Ref. 60(c)]. Results for  $\text{GaAs}_x\text{Sb}_{1-x}$  using model I [Fig. 12(b)] give  $\Omega_{\text{bk}}^H(x = 0.5) \approx 4.9$  kcal/mol, in reasonable agreement with the value 4.0–4.5 found by Stringfellow using the  $\delta$  lattice parameter model.<sup>40</sup> Results for model II [Fig. 12(c)] are significantly higher:  $\Omega_{\text{bk}}^H \approx 6.6$  kcal/mol. [Inclusion of distant-neighbor interactions (using ten equa-

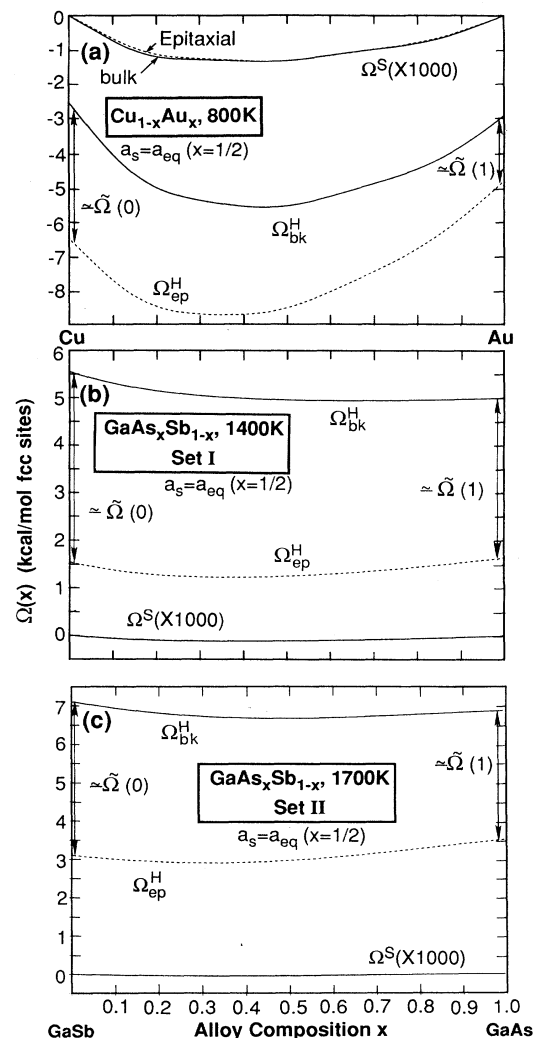


FIG. 12. Interaction parameters  $\Omega$  for bulk mixing enthalpy  $\Omega_{\text{bk}}^H$ , epitaxial mixing enthalpy  $\Omega_{\text{ep}}^H$  [from  $\delta H_{\text{ep}}(x)$ ], and nonrandom entropy for  $\text{Cu}_{1-x}\text{Au}_x$  at 800 K, (a),  $\text{GaAs}_x\text{Sb}_{1-x}$  (model I) at 1400 K, (b), and  $\text{GaAs}_x\text{Sb}_{1-x}$  at 1700 K (model II), (c). Solid and dashed lines indicate bulk and epitaxial (for [001]-oriented substrate with  $a_s = a_{\text{eq}}(0.5)$ ) values, respectively. In (b) and (c) bulk and epitaxial  $\Omega^S$  curves are indistinguishable.

tions of state in the cluster description) determined from LAPW calculations<sup>60(a)</sup> produce good agreement with experiment ( $\Omega_{\text{bk}}^H \approx 4.0$  kcal/mol.) However,  $\tilde{\Omega}$  at  $x=0$  and 1 are almost identical for models I and II, emphasizing that  $E_{\text{ES}}(a_s, x, T)$  [Eq. (3.14)] depends primarily on alloy elastic properties and only very weakly on the parameters  $\Delta H_n$  which distinguish the two models.

### E. Cluster populations

Examination of the cluster probabilities provides insight into how an alloy responds to the epitaxial constraint. For high enough temperatures the cluster probabilities  $P_n(x, T)$  assume their random (R) binomial distribution values. For our choice of clusters  $n=0-4$ ,

$$P_n^R(x, T) = 4! / [(4-n)! n!] x^n (1-x)^{4-n}. \quad (5.11)$$

As  $T$  is reduced the  $P_n$  determined variationally from the cluster variation method depart from the random values, reflecting a thermodynamic enhancement or suppression of the distinct clusters. Figure 13 shows the *excess* clus-

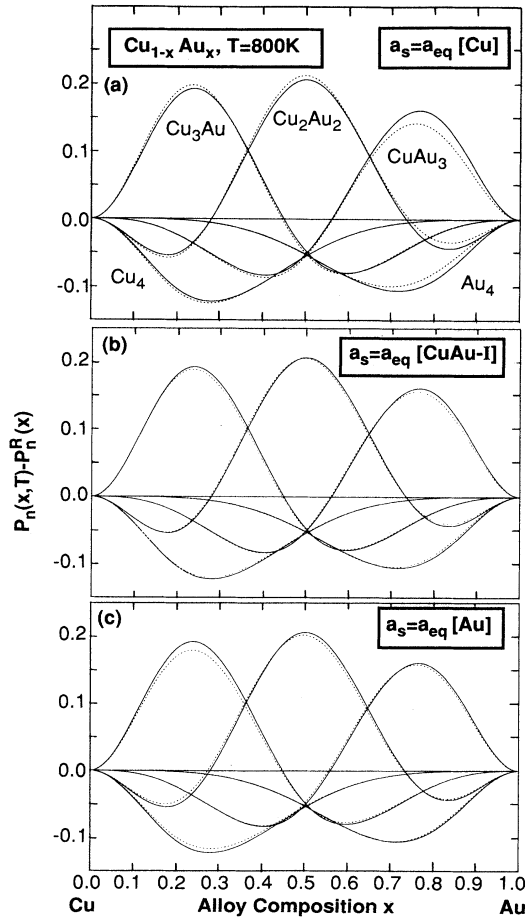


FIG. 13. Deviation from random cluster probabilities for  $\text{Cu}_n \text{Au}_{4-n}$  clusters in disordered bulk (solid lines) and epitaxial (dashed lines)  $\text{Cu}_{1-x} \text{Au}_x$  alloy at 800 K for [001]-oriented substrate with  $a_s = a_{\text{eq}}[\text{Cu}]$ ,  $a_{\text{eq}}[\text{CuAu-I}]$ , and  $a_{\text{eq}}[\text{Au}]$ , (a), (b), and (c), respectively.

ter probabilities  $\Delta P_n(x, T) = P_n(x, T) - P_n^R(x)$  for bulk (solid lines) and epitaxial (dashed lines)  $\text{Cu}_{1-x} \text{Au}_x$  for the three substrates given in Figs. 4 and 7. While the bulk curves are indistinguishable from the anharmonic results of Refs. 60(c) and 60(d), the epitaxy-induced redistribution of cluster probabilities is generally *small over the entire composition range*. At the lattice-matched composition the bulk and epitaxial cluster probabilities are *identical* for all clusters, so that bulk and epitaxial alloys are structurally and energetically indistinguishable.

The  $\epsilon$ - $G$  analysis of Sec. VC may be used to understand these cluster redistributions. For  $\epsilon^{(m)} < 0$ , the probability for cluster  $A_{4-m}B_m$  is *enhanced*<sup>60(e)</sup> over its random value; under epitaxial conditions, if [Eq. (5.10)]  $\Delta \epsilon^{(m)}(a_s) = -\Delta(a_s, x_m) > 0$ , cluster  $m$  will correspondingly be *suppressed* with respect to bulk. Inspection of Fig. 10(a) suggests prominent suppressions near  $x=0.2$  for the  $\text{Cu}_3\text{Au}$  cluster on  $a_s = a_{\text{eq}}[\text{Cu}]$ , and near  $x=0.8$  for  $\text{CuAu}_3$  for  $a_s = a_{\text{eq}}[\text{Au}]$ . These expectations are directly confirmed in Figs. 13(a) and 13(c), respectively.

In Fig. 14(a) we show the  $\Delta P_n(x, T)$  for  $\text{GaAs}_x \text{Sb}_{1-x}$  for  $a_s = a_{\text{eq}}[\text{Ga}_2\text{AsSb}]$  at 1300 K, using model I; results

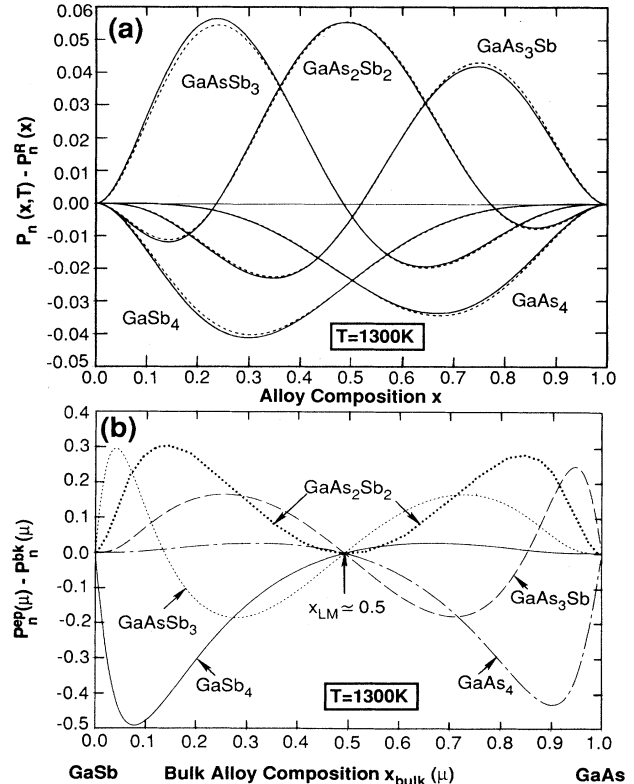


FIG. 14. Excess cluster probabilities for bulk (solid lines) and epitaxial (dashed lines) for  $\text{GaAs}_x \text{Sb}_{1-x}$  alloy (model I) at 1300 K for [001]-oriented substrate with  $a_s = a_{\text{eq}}[\text{Ga}_2\text{AsSb}]$  as a function of alloy composition  $x$ , (a). For fixed growth conditions (chemical potential  $\mu$ ), redistribution of epitaxial cluster probabilities with respect to bulk, (b).  $x_{\text{LM}}$  indicates lattice-matched composition.

using II are similar. Although  $\text{Cu}_{1-x}\text{Au}_x$  has stable clusters ( $\Delta H_n < 0$ ) while  $\text{GaAs}_x\text{Sb}_{1-x}$  does not ( $\Delta H_n > 0$ ), both show enhancement of mixed clusters ( $\epsilon^{(m)} < 0$ ), as discussed in Sec. V C. The  $\epsilon$ - $G$  analysis using Fig. 10(b) predicts [as confirmed in Fig. 14(a)] for  $a_s = a_{\text{eq}}(x=0.5)$  an epitaxial suppression of  $\text{Ga}_4\text{AsSb}_3$  clusters near  $x=0.2$ , and an enhancement of similar magnitude for  $\text{Ga}_4\text{As}_3\text{Sb}$  clusters near  $x=0.8$ . The relatively small values, even smaller than for  $\text{Cu}_{1-x}\text{Au}_x$  because of the higher temperature, disguise an important difference between epitaxial and bulk cluster distributions. A given set of experimental growth conditions corresponds to fixing the chemical potentials of all chemical species present. Thus to compare epitaxial and bulk cluster distributions it is more natural to plot the  $P_n$  as a function of *chemical potential*  $\mu$ . Because of the extremely sensitive dependence of alloy composition on  $\mu$ , we have chosen to display in Fig. 14(b)  $\bar{P}_n(a_s, \mu, T) - P_n(\mu, T)$  as a function of the bulk alloy composition  $x_{\text{bk}}(\mu)$ . This figure makes obvious the large microscopic differences between epitaxial and bulk alloys. While at the lattice-matched composition  $x_{\text{LM}}$  the epitaxial and bulk cluster probabilities are identical, the unstrained  $\text{GaAs}_2\text{Sb}_2$  clusters have been enhanced over the entire composition (or chemical potential) range.

## VI. COMPOSITION PINNING DURING GROWTH OF EPITAXIAL ALLOYS

### A. Thermodynamic description

Previous sections examined the energetics of epitaxially constrained systems and qualitative effects on phase coex-

istence or stabilization. We next examine one of the earliest quantitative effects documented for epitaxial alloys, the tendency of the measured composition  $x_{\text{ep}}$  of the epitaxial alloy to be "pinned" near  $x_{\text{LM}}$ , where the alloy is lattice matched to the substrate, even though the composition  $x_{\text{bk}}$  of the corresponding (unsupported) bulk alloy varies widely.

Wood and Zunger<sup>18</sup> have discussed this effect; we briefly summarize their thermodynamic parametrization for use below. For any phase there is a monotonic relation between the chemical potential  $\mu = d\Delta F/dx$  and the composition  $x$ . We may Taylor expand about  $\mu_{\text{LM}}$  [where  $a(x_{\text{LM}}) = a_s$  and bulk and epitaxial alloys are indistinguishable according to Eq. (3.14)], to find

$$\begin{aligned} \delta x_{\text{bk}}(\mu) &\equiv x_{\text{bk}}(\mu) - x_{\text{LM}} \\ &= (\mu - \mu_{\text{LM}}) / (d^2\Delta F^{\text{bk}}/dx^2)|_{x_{\text{LM}}} + \dots, \end{aligned} \quad (6.1a)$$

$$\begin{aligned} \delta x_{\text{ep}}(\mu) &\equiv x_{\text{ep}}(\mu) - x_{\text{LM}} \\ &= (\mu - \mu_{\text{LM}}) / (d^2\Delta F^{\text{ep}}/dx^2)|_{x_{\text{LM}}} + \dots \end{aligned} \quad (6.1b)$$

using the identity  $dx/d\mu = (d\mu/dx)^{-1} = (d^2\Delta F/dx^2)^{-1}$ . Under identical growth conditions  $\mu$  is common to bulk and epitaxial alloys growing near equilibrium. We may thus conveniently measure the degree of composition pinning at the lattice-matched composition by the slope  $Q(x_{\text{LM}}) \equiv dx_{\text{ep}}/dx_{\text{bk}}$  of the curve  $x_{\text{ep}}(\mu)$  versus  $x_{\text{bk}}(\mu)$  at  $x_{\text{LM}}$ , or

$$Q = [d^2\Delta F^{\text{bk}}(x_{\text{LM}})/dx^2] / \{d^2\Delta F^{\text{ep}}[x_{\text{LM}}, a_s = a(x_{\text{LM}})]/dx^2\}, \quad (6.2)$$

$$Q(x_{\text{LM}}, T) = \frac{T - \tau_{\text{bk}}(x_{\text{LM}})}{T - \tau_{\text{ep}}(x_{\text{LM}})}. \quad (6.3)$$

As described above, a homogeneous disordered phase of a separating alloy such as  $\text{Ga}_{1-x}\text{In}_x\text{As}$  ceases to be stable for temperatures below the spinodal temperature  $\tau(x)$ , whose maximum coincides with the maximum miscibility gap temperature. The spinodal temperature  $\tau(x)$  is the locus of points satisfying  $d^2\Delta F/dx^2 = 0$ ; we demonstrated above (Fig. 12) that the epitaxial constraint strongly modifies  $\Delta H(x)$  while leaving  $\Delta S_{\text{ep}}(x) \simeq \Delta S_{\text{bk}}(x)$ . Thus the epitaxial spinodal temperature  $\tau_{\text{ep}}$  is related to  $\tau_{\text{bk}} = (d^2\Delta H_{\text{bk}}/dx^2)/(d^2\Delta S_{\text{bk}}/dx^2)$  to high precision, using Eq. (3.14), by

$$\begin{aligned} \tau_{\text{ep}}(x_{\text{LM}}) &= [\tau_{\text{bk}}(x) - \frac{3}{4}a(x)q(x)B(x)(da/dx)^2/k_B]_{x_{\text{LM}}} \\ &\equiv \tau_{\text{bk}}(x_{\text{LM}}) + \Delta\tau(x_{\text{LM}}). \end{aligned} \quad (6.4)$$

### B. Composition pinning and epitaxial stabilization

Equations (6.2)–(6.4) connect composition pinning and epitaxial stabilization of alloys. Since  $\Delta\tau \leq 0$ , for any  $T$  above the bulk miscibility-gap temperature  $Q < 1$ , i.e., composition pinning is a *universal* feature of coherent ep-

itaxial growth, even on a lattice-matched substrate. Perfect composition pinning ( $Q=0$ ) occurs at the bulk spinodal temperature  $T = \tau_{\text{bk}}(x)$ , while  $Q \rightarrow 1$  as  $T \rightarrow \infty$ . (While composition pinning may persist below the bulk miscibility temperature, it must do so in some guise other than an  $x_{\text{ep}}$  versus  $x_{\text{bk}}$  plot, since the full range of bulk-alloy composition is inaccessible.) Larché and Cahn<sup>29</sup> explained composition pinning in liquid-phase epitaxy in precisely the same terms, but failed to note the quantitative connection with epitaxial stabilization of alloys ( $\Delta\tau < 0$ ).

Equations (6.3) and (6.4) show that composition pinning and epitaxial stabilization both scale as  $(da/dx)^2 \propto (\Delta a)^2$ , where  $\Delta a$  is the lattice mismatch between the *alloy constituents* (not between substrate and the film material); nearly lattice-matched systems (e.g.,  $\text{Ga}_{1-x}\text{Al}_x\text{As}$ ) will show no epitaxial effects. Both effects are larger for elastically stiff alloys, via  $q(x)B(x)$  and depend on orientation through  $q$ . The physical origin of both is not epitaxial strain *per se* (since both occur even on lattice-matched substrates), but rather the composition dependence of the alloy parameter  $a(x, T)$ , present

either in phenomenological elastic descriptions or in first-principles cluster-based calculations. This dependence obviously may be traced to the size mismatch  $\Delta a$  between alloy constituents, reflecting different atomic sizes or distinct bond lengths and their imperfect accommodation in an alloy environment.

### C. Quantitative results

#### 1. Separating alloys

Using model I data, used to compute the phase diagrams for  $\text{GaAs}_x\text{Sb}_{1-x}$  given in Fig. 8, we show in Fig. 15 CVM results for substrates lattice matched to the alloy at  $x=0$ ,  $x \approx 0.5$ , and  $x=1$  at 1300 K; results for II are expected to be similar (within  $\sim 6\%$ , because of the similar epitaxial suppressions of the miscibility gaps). The epitaxy-induced increase in  $d\mu/dx = d^2\Delta F/dx^2$  (i.e.,  $Q < 1$ ) in Fig. 15(a) is most pronounced at  $x_{\text{LM}} \approx 0.5$ ; a given  $\mu$  (fixed growth conditions) corresponds to different values of  $x_{\text{ep}}$  and  $x_{\text{bk}}$ . Figure 15(b) shows strong deviations from  $x_{\text{ep}} = x_{\text{bk}}$  (i.e.,  $Q = 1$ ) even well away from  $x_{\text{LM}}$  and  $50^\circ\text{C}$  above the calculated maximum bulk miscibility gap temperature ( $\approx 1245\text{ K}$ ). These results are directly

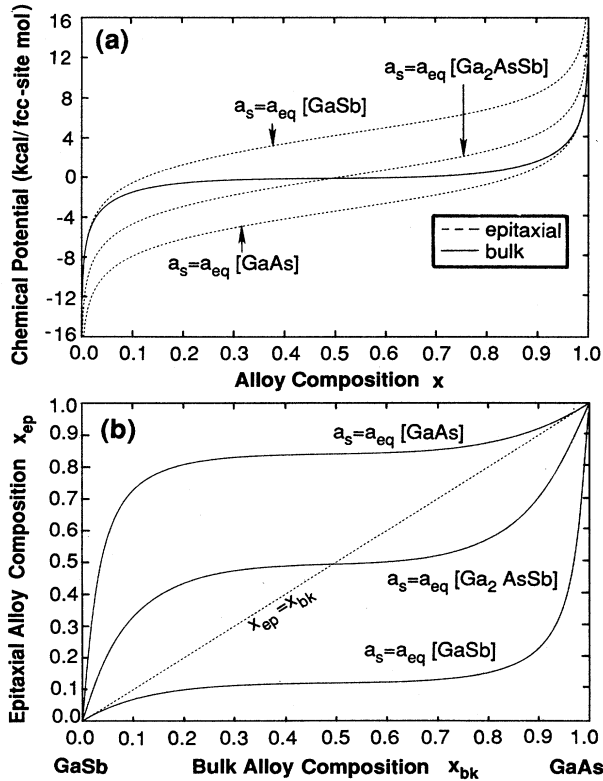


FIG. 15. CVM predictions for bulk and epitaxial  $\text{GaAs}_x\text{Sb}_{1-x}$  (model I): (a) dependence of alloy composition on chemical potential  $\mu$ ; (b)  $x_{\text{ep}}(\mu)$  vs  $x_{\text{bk}}(\mu)$ , exhibiting composition pinning.

relevant to liquid-phase epitaxy and strongly resemble the original curve of Stringfellow.<sup>21</sup>

In Fig. 14(b) (discussed in Sec. V E) we displayed the epitaxy-induced redistribution of cluster probabilities  $\Delta P_n \equiv P_n^{\text{ep}}(\mu) - P_n^{\text{bk}}(\mu)$  versus  $x_{\text{bk}}(\mu)$  on a substrate lattice matched to  $x \approx 0.5$ . Alone among the five clusters, the nearly lattice-matched  $\text{GaAs}_2\text{Sb}_2$  cluster is enhanced ( $\Delta P_n \geq 0$ ) over the entire composition range. In the context of composition pinning we note that the compositions at which the probability redistribution for  $\text{GaAs}_2\text{Sb}_2$  clusters is a maximum correspond roughly to the limits of significant composition pinning in Fig. 15. Figure 14(b) is thus a microscopic manifestation of the phenomenon of composition pinning.

#### 2. Composition pinning in ordering alloys and ordered compounds

The qualitative remarks above hold for ordering [ $\Delta H(x) \leq 0$ , e.g.,  $\text{Cu}_{1-x}\text{Au}_x$ ] or phase-separating [ $\Delta H(x) \geq 0$ , e.g., most isovalent semiconductor] alloys. Since formally the miscibility-gap temperature is negative for ordering alloys, we expect considerably less composition pinning for ordering alloys. In Fig. 16(a) we show composition pinning curves for the disordered  $\text{Cu}_{1-x}\text{Au}_x$  alloy and ordered  $\text{Cu}_{4-n}\text{Au}_n$  compounds at 500 K for a

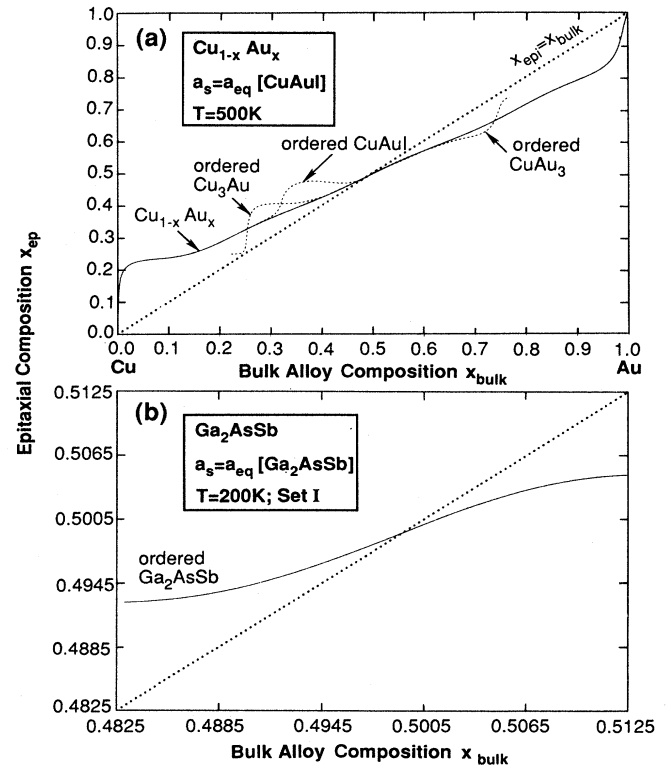


FIG. 16. CVM predictions for composition pinning of ordered compounds:  $\text{Cu}_{4-n}\text{Au}_n$  and  $\text{Cu}_{1-x}\text{Au}_x$ , (a);  $\text{Ga}_2\text{AsSb}$  (model I), (b).

substrate lattice matched to ordered CuAu-I, using CVM results. The slope  $Q$  of these curves is much closer to 1 (no composition pinning) than for  $\text{GaAs}_x\text{Sb}_{1-x}$  curves in Fig. 15. Figure 16(b) gives the composition pinning curve for ordered  $\text{Ga}_2\text{AsSb}$  at 200 K (below the epitaxial spinodal for this composition, so that no comparison with the disordered alloy is possible); the slope  $Q$  at this temperature is considerably less than that for the disordered alloy at  $T = 1400$  K in Fig. 15.

### 3. Phenomenological treatment of epitaxial energetics

At temperatures well above ordering temperatures of possible metastable ordered  $(AC)_m(BC)_{4-m}$  compounds (and provided a random entropy description is adequate), reasonable quantitative results for a variety of isovalent  $A_{1-x}B_xC$  semiconductor alloys can be found using the simple "regular solution model."<sup>40</sup> This approach takes the mixing entropy  $\Delta S(x)$  as strictly random and assumes  $\Delta H(x) = \Omega_{\text{bk}}^H x(1-x)$ , where  $\Omega_{\text{bk}}^H$  is the "interaction parameter" (independent of  $x$  and  $T$ ) of the bulk alloy. As demonstrated in Sec. VD and Fig. 12, the alloy epitaxial strain energy is well described [see Eq. (3.14)] by  $E_{\text{ES}}(a_s, x, T) \approx \tilde{\Omega}(x - x_{\text{LM}})^2$ . Hence within this phenomenological model we find for the spinodals (which coincides with the miscibility gap at its maximum)

$$\tau^{\text{bk}}(x) = (2\Omega_{\text{bk}}^H/R)x(1-x) \quad (6.5)$$

and

$$\tau^{\text{ep}}(x_{\text{LM}}) = [2(\Omega_{\text{bk}}^H - \tilde{\Omega})/R]x_{\text{LM}}(1-x_{\text{LM}}), \quad (6.6)$$

with  $\Omega$  measured per mol and  $R$  the gas constant. Using Eq. (3.14) near  $x_{\text{LM}} = 0.5$  we find

$$\begin{aligned} \tilde{\Omega} &= \frac{9}{8}a(x_{\text{LM}})q(x_{\text{LM}})B(x_{\text{LM}})(da/dx)^2(x_{\text{LM}}) \\ &\approx \frac{9}{8}a_{\text{av}}(qB)_{\text{av}}(\Delta a)^2, \end{aligned} \quad (6.7)$$

where  $\Delta a$  is the lattice mismatch between the alloy constituents and  $\text{av}$  indicates the average of the values for  $x = 0$  and  $x = 1$ . These expressions are useful for estimating the magnitude of epitaxial effects, but if the predicted value of  $\tau^{\text{ep}}$  is comparable to order-disorder transition temperatures of epitaxial phases, strong distortions of the miscibility gap may be expected (see, e.g., Fig. 8). Even in the absence of stable epitaxial phases, there may remain strong asymmetries of the miscibility gap, associated with very different formation enthalpies  $\Delta H_n$  for metastable bulk ordered phases at  $x = 0.25$  and  $x = 0.75$  (see, e.g., Fig. 9). For  $\text{GaAs}_x\text{Sb}_{1-x}$  at  $x_{\text{LM}} = 0.5$ , Table II and Eqs. (6.6), (6.7), and (3.14) predict an epitaxial suppression  $\tau^{\text{ep}} - \tau^{\text{bk}}$  of  $946^\circ\text{C}$  and  $\tilde{\Omega} \approx 3.76$ , in excellent agreement with the CVM values  $953^\circ\text{C}$  (at  $x \approx 0.8$ , reflecting the distortions mentioned) and  $\tilde{\Omega} \approx 3.7$  (Fig. 12), respectively. Here the quantitative agreement between cluster variation results and the simple phenomenological elastic treatment above is due to the fact that CVM-computed alloy elastic properties [e.g.,  $q(x, T)B(x, T)$  and  $c_{\text{eq}}(a_s, x, T)$ ] differ very little from composition-weighted averages of the values for the  $x = 0$  and  $x = 1$  constituents.

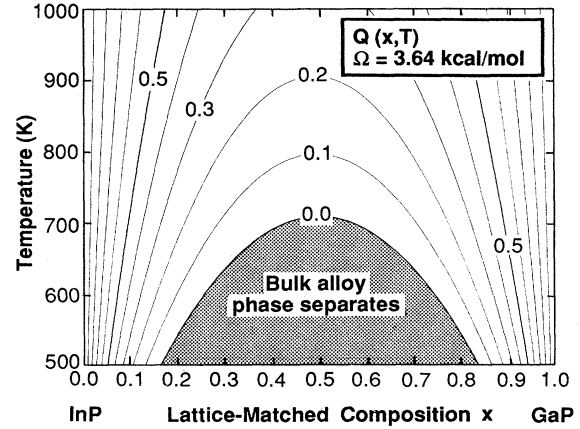


FIG. 17. Regular solution model contours of constant composition pinning  $Q(x, T)$  for epitaxial  $\text{Ga}_x\text{In}_{1-x}\text{P}$  on [111] substrate lattice matched to each composition  $x$ . Shaded area indicates interior of bulk spinodal.

Figure 17 shows contours of constant  $Q(x, T)$  using the regular solution theory for the alloy system  $\text{Ga}_x\text{In}_{1-x}\text{P}$  (with<sup>40</sup>  $\Omega \approx 3.64$  kcal/mol), where it is assumed that for each  $x$  the alloy is grown on a [111] substrate lattice matched to that composition. In this figure the shaded region indicates the interior of the bulk spinodal; we note pronounced composition pinning more than  $300^\circ\text{C}$  above the miscibility gap at  $x \approx 0.5$ , so that proximity to the bulk spinodal is not required. We also note a value for  $Q$  for a lattice-matched value of  $x \approx 0.51$  (used by Stringfellow<sup>21</sup>) of about 0.094, very close to the value calculated by Larché and Cahn<sup>29</sup> and observed<sup>21</sup> at  $800^\circ\text{C}$ .

### D. Relation between epitaxial strain and coherency strain

Epitaxial suppression of miscibility gap temperatures is very closely related to "coherency strain" in bulk alloys. It was observed<sup>46-48</sup> that some bulk pseudobinary  $A_{1-x}B_xC$  semiconductor alloys grown above the bulk spinodal temperature could be quenched to lower temperatures without spinodally decomposing into  $AC$ - and  $BC$ -rich regions. Below the spinodal temperature the homogeneous alloy is thermodynamically unstable with respect to long-wavelength one-dimensional density fluctuations which culminate for long times (in the absence of kinetic barriers) in phase separation. The specific elastic properties of the (e.g., cubic) alloy determine the crystallographic direction along which such fluctuations first occur.

As noted by Cahn,<sup>50</sup> the equilibrium volumes of  $AC$  and  $BC$  in general differ from that of the alloy, so phase separation necessarily raises the alloy strain energy. Cahn demonstrated that this effect suppressed the miscibility-gap temperature by an amount which depended on the direction along which the alloy was elastically softest, as parametrized by what is precisely  $q$  [Eqs. (2.3) and (2.4)] in our notation. Thus the suppression of the bulk miscibility gap due to coherency strain is very similar to that due to epitaxial strain, and will coincide if the

substrate orientation coincides with the direction along which the alloy is elastically softest.

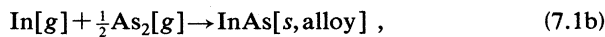
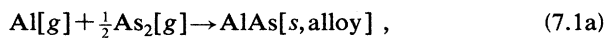
Bulk coherency strain and epitaxial strain differ in one important respect. The former manifests itself only *below* the (unmodified) bulk miscibility-gap temperature, while the latter has effects for *all* temperatures below melting. The theory of composition pinning given in Sec. VI A depends explicitly on both the bulk and epitaxial spinodal temperatures. To the extent that it did account *quantitatively* for measured values of  $Q(x, T)$  for temperatures greater than the bulk miscibility gap (where LPE growth is typically carried out) there is no need to invoke any modifications of  $T_{MG}^{bk}$  due to coherency strain for  $T > T_{MG}^{bk}$ .

## VII. EPITAXIAL EFFECTS IN MOLECULAR-BEAM EPITAXY GROWTH

### A. Thermodynamic description

Molecular-beam epitaxy (MBE) is frequently regarded as a nonequilibrium or kinetically controlled process. However, recent work<sup>75-78</sup> suggests that provided the actual reactions occurring are known and characterized by their thermodynamic variables, an equilibrium thermodynamic analysis can account for observed growth rates and other properties of epitaxial alloys. Seki and Koukitu<sup>77</sup> (SK) have recently given such an analysis of molecular-beam epitaxy growth of bulk III-V pseudobinary alloys, neglecting the strain effects of coherent epitaxy we have considered above. They note that MBE growth rates are roughly independent of beam temperature and limited by the incident flux of group-III atoms. Because surface migration of adatoms and succeeding chemical reactions are rapid on the scale of the group-III-atom arrival rate, they note that chemical equilibrium is established at the substrate surface and use a simplified Hertz-Knudsen equation for the growth rate  $r$ , i.e.,  $r \simeq k(P_{III}^{ap} - P_{III})$ , where  $k$  is a constant and  $P_{III}^{ap}$  and  $P_{III}$  are the applied and equilibrium partial pressures of the group-III atom. The approach of SK consists of three steps: (i) identifying the net effective chemical reactions for incorporation of vapor-phase reactants into a solid-phase alloy and characterizing each by a temperature-dependent equilibrium constant; (ii) requiring that group-III and -V atoms be incorporated at the same rate, and (iii) finding the steady-state alloy composition corresponding to a given set of growth parameters. In this section we generalize their approach to include explicitly the effects of epitaxial strain. We illustrate this approach with a calculation for  $Al_x In_{1-x} As$ , for which considerable experimental data exists.<sup>26,62,78</sup>

The relevant reactions when  $As_4$  is used as the As source according to SK are



where  $g$  indicates a gas-phase reactant and "s, alloy" indicates that the product is in the solid-phase alloy environ-

ment. These equations may be rewritten in terms of equilibrium constants and equilibrium partial pressures (in atmospheres) of the vapor-phase reactants as

$$a_{AlAs}(x, T)/(P_{Al}P_{As_2}^{1/2}) = K_{Al}(T), \quad (7.2a)$$

$$a_{InAs}(x, T)/(P_{In}P_{As_2}^{1/2}) = K_{In}(T), \quad (7.2b)$$

$$P_{As_2}^2/P_{As_4} = K_{As}(T), \quad (7.2c)$$

where the  $a$ 's are activities of the solid phase, discussed further below. The equilibrium constants  $K$  depend only on temperature, and are generally well represented in the form  $K(T) = 10^{b+c/T}$  with  $T$  the temperature in K. For the reaction (7.2c), for example,  $b = 7.470$  and  $c = -13.30 \times 10^3$ .

Physical growth conditions are specified by the substrate temperature  $T$  and the applied partial pressures  $P_\alpha^{ap}$  of the reactants. The unknowns of the problem are the equilibrium partial pressures of the reactants (four parameters, including  $As_4$ ) and the steady-state alloy composition (a fifth parameter). Defining  $z = a_{AlAs}/K_{Al}P_{Al}$ , we find  $P_{Al} = a_{AlAs}/zK_{Al}$ ,  $P_{In} = a_{InAs}/zK_{In}$ ,  $P_{As_2} = z^2$ , and  $P_{As_4} = z^4/K_{As}$ . Within the simplified model of SK the growth rate  $r_\alpha$  of species  $\alpha$  is given by  $r_\alpha = k(P_\alpha^{ap} - P_\alpha)$  with  $k$  a constant. A fourth equation

$$(4/K_{As})z^4 + 2z^2 - (a_{AlAs}/K_{Al} + a_{InAs}/K_{In})/z - (P_{As}^{ap} - P_{Al}^{ap} - P_{In}^{ap}) = 0 \quad (7.3)$$

results from requiring that the total group-III (In+Al) growth rate be the same as the total group-V (As) growth rate. Experimentally As is introduced into the reaction chamber as  $As_4$  at temperatures low enough that the dimer concentration is small, so that we assume the nominal applied As pressure is given by  $P_{As}^{ap} \simeq 4P_{As_4}^{ap}$ .

The solution of Eq. (7.3) depends on the alloy composition  $x$  and substrate temperature  $T$  through the activities  $a_{AlAs}$  and  $a_{InAs}$ . The activity for species  $\beta$  is defined by

$$a_\beta(x, T) = \exp \left[ \frac{\partial}{\partial N_\beta} \sum_\alpha N_\alpha \Delta G_{mix}(x, T) / k_B T \right], \quad (7.4)$$

where  $N_\beta$  is the number of moles of species  $\beta$  in the alloy and  $\Delta G_{mix} = \Delta H - T\Delta S_{mix}$  is the alloy free energy of mixing, with  $k_B$  Boltzmann's constant. If for  $Al_x In_{1-x} As$  we define the composition as  $x = N_1 / (N_1 + N_2)$ , then, using the identities  $d/dN_\alpha = \partial/\partial N_\alpha + (dx/dN_\alpha)\partial/\partial x$ ,  $dx/dN_1 = (1-x)/(N_1 + N_2)$ , and  $dx/dN_2 = -x/(N_1 + N_2)$  we find

$$a_{AlAs} = \exp \{ [\Delta G_{mix} + (1-x)d\Delta G_{mix}/dx] / k_B T \}, \quad (7.5a)$$

$$a_{InAs} = \exp [(\Delta G_{mix} - x d\Delta G_{mix}/dx) / k_B T]. \quad (7.5b)$$

If  $\Delta G_{mix}(x, T)$  is known the activities can be calculated directly. For simplicity in describing pseudobinary isovalent semiconductor alloys (following SK) we take  $\Delta S_{mix}$  to be the random value  $-k_B[x \ln x + (1-x)\ln(1-x)]$  and for the bulk alloy enthalpy of mixing we adopt the regular solution model used to illustrate composition pinning in Fig. 17, using a value of  $\Omega_{bk}^H$  tabulated by String-

fellow.<sup>40</sup> For a coherent *epitaxial* alloy (not treated by SK) we may use Eq. (3.14) to evaluate the contribution  $\Delta E_{ES}(x, a_s)$  due to the epitaxial constraint. Then

$$a_{\text{AlAs}}(x, T) = \{x \exp[\Omega_{\text{bk}}^H(1-x)^2/k_B T]\} \\ \times \exp[E_{ES}(x, a_s) + (1-x)dE_{ES}(x, a_s)/dx], \quad (7.6a)$$

$$a_{\text{InAs}}(x, T) = [(1-x)\exp(\Omega_{\text{bk}}^H x^2/k_B T)] \\ \times \exp[E_{ES}(x, a_s) - x dE_{ES}(x, a_s)/dx]. \quad (7.6b)$$

In curly braces are the activities of the corresponding *bulk* alloy (identical to those used by SK); the trailing exponentials reflect contributions due to coherent epitaxy. For the calculations below we assume, as do Seki and Koukitu for the bulk case, that  $q(x)B(x)$  and  $a(x)$  are simple weighted averages of the values for pure InAs ( $x=0$ ) and AlAs ( $x=1$ ). The parameters used are given<sup>78</sup> in Table VI.

With the activities now explicitly known for given composition  $x$  of a bulk or epitaxial alloy, we may solve for the physically relevant positive real root  $z^*$  of Eq. (7.3). From  $z^*$  we can find the equilibrium partial pressures, as described above, and calculate the physically measurable "incorporation coefficients"  $\alpha_\beta = 1 - P_\beta/P_\beta^{\text{ap}}$ ; a positive value of  $\alpha$  corresponds to a *growing* alloy. There is no guarantee that, e.g., the equilibrium pressure  $P_{\text{In}}$  found above will yield a positive value of  $\alpha_{\text{In}}$ , however. To avoid this problem one may solve for the *steady-state* alloy composition by requiring that the growth rates  $r_\beta = k(P_\beta^{\text{ap}} - P_\beta) = k\alpha_\beta P_\beta^{\text{ap}}$  for Al and In reflect the relative proportions in the  $\text{Al}_x\text{In}_{1-x}\text{As}$  alloy, i.e.,

$$r_{\text{AlAs}}/r_{\text{InAs}} = \alpha_{\text{Al}} P_{\text{Al}}^{\text{ap}}/\alpha_{\text{In}} P_{\text{In}}^{\text{ap}} = x/(1-x). \quad (7.7)$$

Equations (7.3) and (7.7) are solved self-consistently to yield the equilibrium partial pressures and the steady-state alloy composition for a specified substrate temperature and applied partial pressures of the reactants. For the  $\text{Al}_x\text{In}_{1-x}\text{As}$  alloy system over the common experimental temperature range  $500 < T < 700^\circ\text{C}$  the equilibrium constant  $K_{\text{Al}}$  is such that  $\alpha_{\text{Al}}$  is almost exactly unity over the entire composition range. Hence, defining the vapor-phase composition  $x_{\text{vap}} = P_{\text{Al}}^{\text{ap}}/(P_{\text{Al}}^{\text{ap}} + P_{\text{In}}^{\text{ap}})$ , Eq. (7.7) yields the approximate relation

$$\alpha_{\text{In}}(x) \simeq [x_{\text{vap}}/(1-x_{\text{vap}})](1-x)/x \quad (7.8)$$

(not used in the results described below). At low temperatures there is no significant desorption of In from the alloy ( $\alpha_{\text{In}} = 1$ ) and  $x = x_{\text{vap}}$ . At temperatures near the bulk In sublimation temperature

$$T_{\text{sub}}(K) \simeq c_{\text{InAs}}/\{-b_{\text{InAs}} + 13.47$$

$$-\log_{10}[P_{\text{III}}^{\text{ap}}(P_{\text{V}}^{\text{ap}} - P_{\text{III}}^{\text{ap}})^{1/2}]\}, \quad (7.9)$$

(valid for low  $x_{\text{vap}}$ ) the more volatile In begins to desorb from the bulk alloy (i.e., its equilibrium partial pressure becomes comparable to the applied pressure), causing  $\alpha_{\text{In}}$  to drop below 1 and the steady-state In atomic fraction  $1-x$  to drop. Thus only alloy compositions  $x \geq x_{\text{vap}}$  are

accessible as the temperature of the substrate is raised. In Eq. (7.9)  $b$  and  $c$  are the coefficients in the exponent of the equilibrium constant for InAs incorporation (Table VII) and  $P_{\text{III}}^{\text{ap}}$  and  $P_{\text{V}}^{\text{ap}}$  are the total applied partial pressures of group-III and group-V elements, in units of  $10^{-6}$  Torr.

## B. Results for $\text{Al}_x\text{In}_{1-x}\text{As}$

To contrast bulk and epitaxial MBE growth, we show in Fig. 18 predictions of the elastic thermodynamic model for epitaxial  $\text{Al}_x\text{In}_{1-x}\text{As}$  alloys on an InP substrate of [001] orientation, for which the lattice-matched composition  $x_{\text{LM}} \simeq 0.48$ . Physical input parameters for the con-

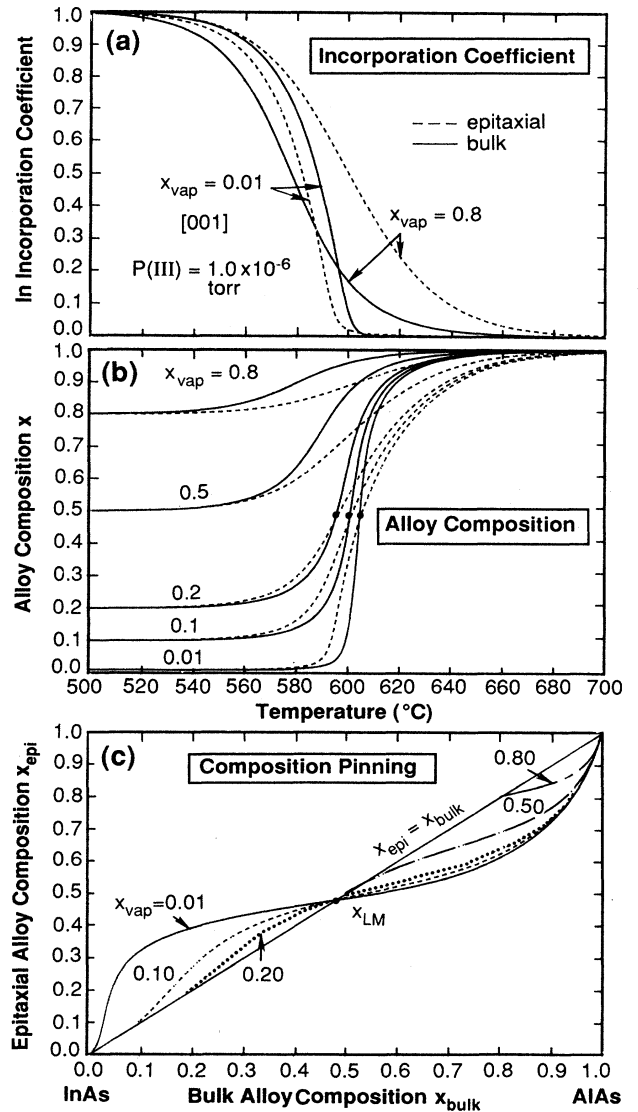


FIG. 18. Predictions of elastic thermodynamic model for MBE growth of  $\text{Al}_x\text{In}_{1-x}\text{As}$  on [001] InP substrate: (a) In incorporation coefficient and (b) steady-state alloy composition, and (c) composition pinning, for various values of vapor composition  $x_{\text{vap}}$ . Heavy dots indicate lattice-matched composition. Data taken from Refs. 77 and 78.

TABLE VI. Equilibrium lattice parameter  $a_{\text{eq}}$  (Å) and cubic elastic moduli  $C_{ij}$  (GPa) used for elastic thermodynamic description of MBE growth of  $\text{Al}_x\text{In}_{1-x}\text{As}$ . Interaction parameter  $\Omega = 2.4964$  kcal/mol. Data taken from Ref. 78.

	$a_{\text{eq}}$	$C_{11}$	$C_{12}$	$C_{44}$
AlAs	5.6622	120.2	57.0	58.9
InAs	6.0584	86.5	48.5	39.6

stituents are given in Table VI; the parameters of the equilibrium constants for reactions Eqs. (7.2a) and (7.2b) are given in the first two rows of Table VII. Figure 18(a) shows the In incorporation coefficient under bulk and epitaxial conditions for two different vapor-phase compositions  $x_{\text{vap}}$ , but with the same net group-III applied pressure  $P_{\text{III}}^{\text{ap}} = 1 \times 10^{-6}$  Torr and  $P^{\text{ap}} = 5 \times 10^{-6}$  Torr. Over this temperature range the Al incorporation coefficient, as mentioned above, differs imperceptibly from 1. Figure 18(b) shows the bulk and epitaxial steady-state alloy compositions for a variety of  $x_{\text{vap}}$  values. In all cases at  $x_{\text{LM}}$  bulk and epitaxial curves coincide, but there are significant modifications away from  $x_{\text{LM}}$ . In Fig. 18(c) we display composition pinning curves, obtained by plotting the steady-state alloy composition  $x_{\text{bk}}$  of the bulk alloy against that for the coherent epitaxial alloy  $x_{\text{ep}}$ . Unlike the CVM results shown in Fig. 15, which are directly relevant to experimental liquid-phase epitaxy (LPE) results, the degree of composition pinning in MBE depends on an external constraint, i.e., the vapor-phase composition  $x_{\text{vap}}$ . Increasing the total applied group-III pressure while keeping  $x_{\text{vap}}$  fixed (not shown) results in a rigid shift of the curves in Figs. 18(a) and 18(b) to higher temperatures. Our calculations (not shown) give an ordering of composition pinning  $Q[111] \lesssim Q[110] < Q[001]$ , as expected from the orientation dependence of the epitaxial elastic modulus  $q$  given in Eqs. (2.3) and (2.4).

Not all experiments on the  $\text{Al}_x\text{In}_{1-x}\text{As}$  epitaxial system correspond to varying the substrate temperature for fixed applied reactant partial pressures. Recent work by Allovon *et al.*<sup>26</sup> corresponds instead to fixing the substrate temperature and scanning the applied partial pressure of In. Here composition pinning appears in another guise, in that<sup>26</sup> "... indium incorporation adjusts itself to compensate a small excess or shortage in the incident

TABLE VII. Constants  $b$  and  $c$  in equilibrium constants  $\log_{10}(K) = b + c/(TK)$  for solid-state incorporation reactions relevant to MBE growth of  $\text{Al}_x\text{In}_{1-x}\text{As}$ .

Compound	$b$	$c$
AlAs <sup>a</sup>	-11.46	$27.67 \times 10^3$
InAs <sup>a</sup>	-11.06	$21.17 \times 10^3$
InAs <sup>b</sup>	-13.79	$21.05 \times 10^3$
InAs <sup>c</sup>	-9.88	$21.17 \times 10^3$

<sup>a</sup>From graphical fit to Fig. 7 of Ref. 77.

<sup>b</sup>C. Chatillon, quoted in Ref. 26.

<sup>c</sup> $b$  chosen to reproduce peak temperature for  $\alpha_{\text{II}}(T) - \alpha_{\text{III}}(T)$  for data sets II and III of Ref. 62.

In flux, in order to ensure perfect lattice matching with the substrate."

### C. Comparison with experiment

The In incorporation coefficient  $\alpha_{\text{In}}(T)$  has been measured for  $\text{Al}_x\text{In}_{1-x}\text{As}$  for a variety of applied pressures and for two different substrates by Turco, Guillaume, and Massies<sup>78</sup> (also discussed by Mbaye *et al.*<sup>62</sup>). These authors give the applied partial pressures of In and As<sub>4</sub> for InP and GaAs substrates and the nominal alloy composition at 500°C. At this temperature the alloy composition satisfies  $x \simeq x_{\text{vap}}$  [see Fig. 18(b)], so that the applied Al partial pressure may be deduced via  $P_{\text{Al}}^{\text{ap}} = [x_{\text{vap}} / (1 - x_{\text{vap}})] P_{\text{In}}^{\text{ap}}$ . The applied pressures determined in this way are given in Table VIII; we have taken  $P_{\text{As}}^{\text{ap}} \simeq 4P_{\text{As}_4}^{\text{ap}}$

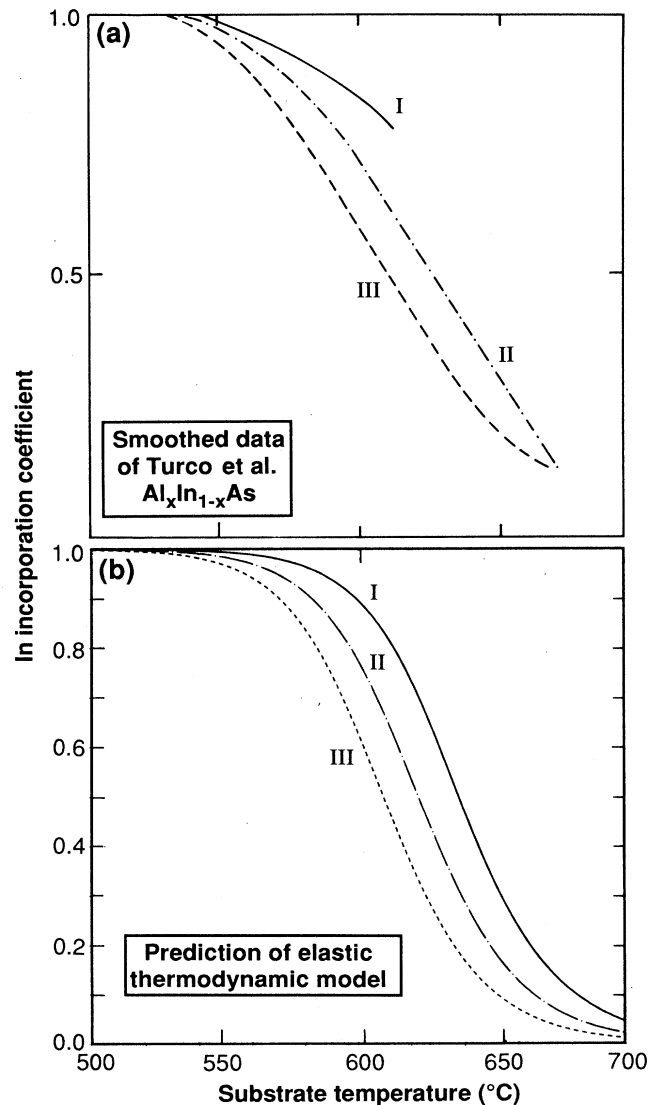


FIG. 19. Comparison of elastic thermodynamic model predictions with measured values of In incorporation coefficient; data sets I–III (after Ref. 78) are described in Table VIII.

TABLE VIII. Experimental conditions for data sets I–III of Turco, Guillaume, and Massies (Ref. 78). Partial pressures in units of  $10^{-6}$  Torr.

Set	[001] substrate	$P_{\text{In}}^{\text{ap}}$	$P_{\text{Al}}^{\text{ap}}$	$P_{\text{As}}^{\text{ap}} = 4P_{\text{As}_4}^{\text{ap}}$
I	InP	0.16	0.148	92
II	GaAs	0.16	0.373	92
III	GaAs	0.08	0.187	92

at the low temperatures where the  $\text{As}_4$  pressures were measured. The corresponding experimental curves  $\alpha_{\text{In}}(T)$  are shown in Fig. 19(a).

The elastic thermodynamic description above is readily applied to predict these curves. The values of  $b$  and  $c$  in the simple expression  $\log_{10}[K(T)] = b + c/T(\text{K})$  are given in Table VII. The values determined from the figures of Seki and Koukitu<sup>77</sup> lead to what is essentially a rigid shift to lower temperatures of the point where  $\alpha_{\text{In}}(T)$  begins to depart from one. Moreover, in comparing recent parametrizations<sup>26,77</sup> of  $K_{\text{In}}$  for InAs (Table VII) one notes a large uncertainty in the value for  $b$  (corresponding to variation in  $K_{\text{In}}$  by a factor of  $\sim 550$ ), which translates into a large uncertainty in the temperature at which In begins to desorb from InAs. To compare with the data of Turco *et al.* we have thus selected a value of  $b$  (Table VII) which reproduces the temperature at which the curve  $\alpha_{\text{II}}(T) - \alpha_{\text{III}}(T)$  (Fig. 20) is a maximum, corresponding to a shift of  $50^\circ\text{C}$  with respect to that found using the SK value for  $b$ . This adjustment leaves the function value  $\alpha_{\text{II}} - \alpha_{\text{III}}$  unchanged (to within 0.3% at its maximum), suggesting this to be a reasonable procedure. With this single adjustment, agreement between the theoretical curves in Fig. 19(b) and the smoothed experimental curves in Fig. 19(a) is quite satisfactory, although the theoretical curves drop more quickly with temperature. In Fig. 20 we show the predictions for  $\alpha_{\text{II}}(T) - \alpha_{\text{III}}(T)$  for the epitaxial alloy and a bulk alloy (with the coherency constraint completely lifted), together with the smoothed experimental data (solid circles).

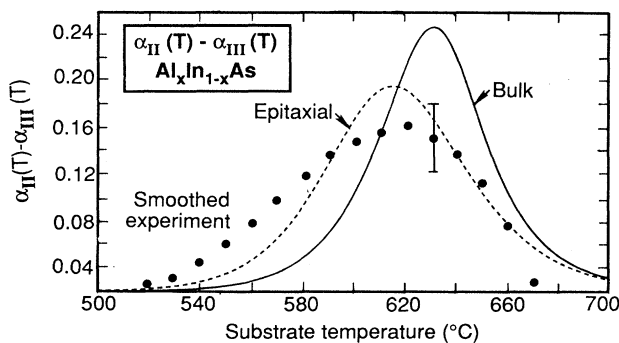


FIG. 20. Elastic thermodynamic model prediction for  $\alpha_{\text{II}} - \alpha_{\text{III}}$  with epitaxial constraint (dashed line) and without ("bulk," solid line), compared with experiment (solid circles and error bar after Ref. 62).

Once again the agreement is quite satisfactory given the uncertainties in the input parameters of the calculation and the sizable error bars of the experiment. The similarity of epitaxial and bulk curves indicates that most features of  $\alpha_{\text{II}} - \alpha_{\text{III}}$  are determined by the differing growth parameters rather than by coherent epitaxial effects, however. Our quantitative results agree with experiment at least as well as those of Ref. 62, without the need for *ad hoc* adjustments of alloy parameters which are a consequence of the incorrect cluster description adopted there.

## VIII. SUMMARY AND CONCLUSIONS

The microscopic cluster-based framework described above, together with a means for variationally determining cluster probabilities, permits detailed comparison of bulk and epitaxial phase diagrams, excess thermodynamic functions, and microscopic cluster properties on a conceptually identical footing. Cluster-variation method calculations were presented for two archetypal alloy systems,  $\text{Cu}_{1-x}\text{Au}_x$  (a typical ordering alloy) and  $\text{GaAs}_x\text{Sb}_{1-x}$  (a typical phase-separating system). Under epitaxial conditions there can be pronounced modifications with respect to bulk of order-disorder transitions and regions of phase stability (for ordering systems), and enormous suppressions of miscibility-gap temperatures with epitaxial stabilization of ordered compounds (for typical phase-separating systems). A strain energy functional theory was given which captures these effects semiquantitatively without the need for CVM calculations. The universal epitaxial phenomenon of composition pinning was characterized thermodynamically and parametrized in terms of bulk and epitaxial spinodal temperatures. These effects were all traced not to lattice mismatch between an alloy and its substrate (since all exist even on substrates lattice matched to the alloy), but to the microscopic mismatch between the alloy constituents. Finally, a thermodynamic analysis of the molecular-beam epitaxy growth of  $A_{1-x}B_xC$  semiconductor alloys which explicitly accounts for the effects of coherent epitaxy was presented and compared with available experimental data.

While the present theory accounts for a variety of experimentally observed effects, its principal shortcoming stems from its fundamentally three-dimensional description of the nature and quantitative details of ordered epitaxial compounds. Isovalent semiconductors  $AC$  and  $BC$  are commonly observed to order into a CuPt-like  $ABC_2$  compound, a structure which under equilibrium three-dimensional conditions should be the least likely to occur (because of its high bulk or epitaxial formation enthalpy). It seems likely that the presence of a free surface at which actual epitaxial film growth occurs catalyzes this CuPt ordering.

## ACKNOWLEDGMENTS

We thank L. G. Ferreira for many useful discussions, S.-H. Wei and J. Bernard for providing first-principles data on the  $\text{GaSb}_{4-n}\text{As}_n$  compounds (Ref. 41), Dr. Gene

Blakeslee for bringing our attention to the phenomenon of composition pinning and early references, and Dr. Jerry Olson for discussions about MBE growth.

#### APPENDIX: ELASTIC THEORY OF CRITICAL THICKNESSES

Conventional treatments<sup>38</sup> of critical thickness effects assume that the misfit  $f \equiv (a_s - a_{eq})/a_{eq}$  between a material (of equilibrium lattice parameter  $a_{eq}$ ) grown as an epitaxial film (fm) and a substrate (s) (of equilibrium lattice parameter  $a_s$ ) is accommodated by a combination of uniform elastic strain  $\epsilon$  and a two-dimensional grid of misfit dislocations lying in the substrate-film interface. The strain energy per unit film area is resolved into a dislocation contribution linear in  $\epsilon$  and an elastic contribution quadratic in  $\epsilon$ . On minimizing with respect to  $\epsilon$ , one finds that for film thicknesses  $h$  less than the critical thickness

$$h_c = \frac{G_s b}{4\pi f (G_s + G_{fm})(1 + \nu_{fm})} [1 + \ln(h_c/b)], \quad (A1)$$

all of the misfit is accommodated elastically, i.e.,  $\epsilon = f$ . For  $h > h_c$ , a fraction

$$\chi = [1 + \ln(h/b)] / [1 + \ln(h_c/b)] h_c / h \quad (A2)$$

is accommodated elastically, with the remainder taken up by misfit dislocations, of Burgers vector  $b \simeq a_{eq}/\sqrt{2}$ . Here  $G$  is an elastic modulus [see Eq. (2.14)] and  $\nu = (1 + C_{11}/C_{12})^{-1}$  is the Poisson ratio. The elastic energy per unit area is proportional to  $h$ , but so is the number of atoms in the film, so the energy per atom of the uniformly strained film is a constant for  $h < h_c$ . To convert to energy per fcc site (used in the text) we multiply the energy per unit area by  $a_{eq}^3/4h$ , the area of the film per fcc site to lowest order in distortions. This yields Eqs. (2.5) and (2.6) of the text.

<sup>1</sup>A. Zunger and D. M. Wood, *J. Cryst. Growth* (to be published).

<sup>2</sup>For ternary CuPt ordering, see T. Suzuki, A. Gomyo, and S. Iijima, *J. Cryst. Growth* **93**, 396 (1988); A. Gomyo, T. Suzuki, and S. Iijima, *Phys. Rev. Lett.* **60**, 2645 (1988); M. A. Shahid and S. Mahajan, *Phys. Rev. B* **38**, 1344 (1988); S. McKernan, B. C. DeCooman, C. B. Carter, D. P. Bour, and J. R. Shealy, *J. Mater. Res.* **3**, 406 (1988); M. Kondow, H. Kakiyayashi, and S. Minagawa, *J. Cryst. Growth* **88**, 291 (1988); P. Bellon, J. P. Chevalier, G. P. Martin, E. Dupont-Nivet, C. Thiebaut, and J. P. André, *Appl. Phys. Lett.* **52**, 567 (1988); S. R. Kurtz, J. M. Olson, and A. Kibbler, *Solar Cells* **24**, 307 (1988); J. P. Goral, M. M. Al-Jassim, J. M. Olson, and A. Kibbler, *Epitaxy of Semiconductor Layered Structures*, MRS Conf. Proc. Vol. 102, edited by R. T. Tung, L. R. Dawson, and R. L. Gunshor (Materials Research Society, Pittsburgh, 1988), p. 583.

<sup>3</sup>For chalcopyrite ordering, see H. R. Jen, M. J. Cherng, and G. B. Stringfellow, *Appl. Phys. Lett.* **48**, 1603 (1986); H. R. Jen, M. J. Jou, Y. T. Cherng, and G. B. Stringfellow, *J. Cryst. Growth* **85**, 175 (1987); H. R. Jen, M. J. Cherng, M. J. Jou, and G. B. Stringfellow, in *GaAs and Related Compounds, 1986*, Inst. Phys. Conf. Proc. Ser. No. 83, edited by W. T. Lindley (IOP, London, 1987), p. 159.

<sup>4</sup>For ternary CuAu-I ordering, see Ref. 3 and T. S. Kuan, W. I. Wang, and E. L. Wilkie, *Appl. Phys. Lett.* **51**, 51 (1987); T. S. Kuan, T. F. Kuech, W. I. Wang, and E. L. Wilkie, *Phys. Rev. Lett.* **54**, 201 (1985).

<sup>5</sup>For famatinite ordering, see H. Nakayama and H. Fujita, in *GaAs and Related Compounds*, Inst. Phys. Conf. Proc. Ser. No. 79, edited by M. Fujimoto (IOP, London, 1986), p. 289.

<sup>6</sup>A. Ourmazd and J. C. Bean, *Phys. Rev. Lett.* **55**, 765 (1985).

<sup>7</sup>(a) A. A. Mbaye, D. M. Wood, and A. Zunger, *Phys. Rev. B* **37**, 3008 (1988); (b) *Appl. Phys. Lett.* **49**, 782 (1986).

<sup>8</sup>(a) J. L. Martins and A. Zunger, *Phys. Rev. Lett.* **56**, 1400 (1986); *J. Mater. Res.* **1**, 523 (1986); (b) S.-H. Wei and A. Zunger, *Phys. Rev. B* **39**, 3279 (1989).

<sup>9</sup>W. Kümmerle and U. Gradmann, *Solid State Commun.* **24**, 33 (1977); C. Rau, C. Schneider, G. Xing, and K. Jamison, *Phys. Rev. Lett.* **57**, 3221 (1986).

<sup>10</sup>W. Keune, R. Halbauer, U. Gonser, J. Lauer, and D. L. Williamson, *J. Appl. Phys.* **48**, 2976 (1977); M. Onellion, M. A.

Thompson, J. L. Erskine, C. B. Duke, and A. Paton, *Surf. Sci.* **179**, 219 (1987).

<sup>11</sup>J. G. Wright, *Philos. Mag.* **24**, 217 (1971).

<sup>12</sup>M. Mattern and H. Lüth, *Surf. Sci.* **126**, 502 (1983); A. Ritz and H. Lüth, *Phys. Rev. B* **32**, 6596 (1985).

<sup>13</sup>R. F. C. Farrow, D. S. Robertson, G. M. Williams, A. G. Cullis, G. R. Jones, I. M. Young, and P. N. J. Dennis, *J. Cryst. Growth* **54**, 507 (1981). See also R. F. C. Farrow, *J. Vac. Sci. Technol. B* **1**, 222 (1983).

<sup>14</sup>S. Minomura, O. Shimomura, K. Asaumi, H. Oyanagi, and K. Takemura, in *Proceedings of the 7th International Conference on Amorphous and Liquid Semiconductors*, edited by W. E. Spear (University of Edinburgh, Edinburgh, 1977), p. 53.

<sup>15</sup>M. J. Jou, Y. T. Cherng, H. R. Jen, and G. B. Stringfellow, *Appl. Phys. Lett.* **52**, 549 (1988).

<sup>16</sup>R. M. Cohen, M. M. Cherng, R. E. Benner, and G. B. Stringfellow, *J. Appl. Phys.* **57**, 4817 (1985).

<sup>17</sup>D. M. Wood and A. Zunger, *Phys. Rev. Lett.* **61**, 1501 (1988).

<sup>18</sup>D. M. Wood and A. Zunger, *Phys. Rev. B* **38**, 12756 (1988).

<sup>19</sup>P. W. Sullivan, R. F. C. Farrow, and G. R. Jones, *J. Cryst. Growth* **60**, 403 (1982).

<sup>20</sup>A. K. Sood, K. Wu, and J. N. Zemel, *Thin Solid Films* **48**, 73 (1978); **48**, 87 (1978); A. K. Sood and J. N. Zemel, *J. Appl. Phys.* **49**, 5292 (1978).

<sup>21</sup>G. B. Stringfellow, *J. Appl. Phys.* **43**, 3455 (1972).

<sup>22</sup>H. Beneking, N. Grote, P. Mischel, and G. Schulz, in *GaAs and Related Compounds 1974*, Inst. Phys. Conf. Proc. Ser. No. 24, edited by J. Bok (IOP, London, 1975), p. 113.

<sup>23</sup>M. Quillec, H. Launois, and M. C. Joncour, *J. Vac. Sci. Technol. B* **1**, 238 (1983). See also A. Marbeuf and J. C. Guillaume, *J. Phys. (Paris) Colloq.* **43**, C5-47 (1982).

<sup>24</sup>G. A. Antypas and R. L. Moon, *J. Electrochem. Soc.* **121**, 416 (1974).

<sup>25</sup>H. Asai and K. Oe, *J. Cryst. Growth* **62**, 67 (1983).

<sup>26</sup>M. Allovon, J. Primot, Y. Gao, and M. Quillec (unpublished).

<sup>27</sup>The existence of composition pinning in LPE growth was at first disputed (Ref. 28) because at room temperature  $\Delta a_1/a_s = (c_{eq} - a_s)/a_s$  depended strongly on liquid composition so that, were  $x_{ep}$  proportional to  $\Delta a_1/a_s$ , it would not appear pinned. However, Larché and Cahn (Ref. 29) and Joncour *et al.* (Ref. 30) showed that one should relate  $x_{ep}$  to  $\Delta a_1/a_s$  only after (i) the epitaxially strained quantity  $\Delta a_1/a_s$ ,

- is converted to  $[a(x) - a_s]/a_s$ , the unstrained value, and (ii) one corrects for extra strain introduced by cooling from growth to room temperature. The magnitude of  $\Delta a_1/a_s$  is then consistent with composition pinning.
- <sup>28</sup>M. Kume, J. Ohta, N. Ogasawara, and R. Ito, *Jpn. J. Appl. Phys.* **21**, L424 (1982); H. Asai and K. Oe, *J. Appl. Phys.* **53**, 6849 (1982); K. Oe, Y. Shinoda, and K. Sugiyama, *Appl. Phys. Lett.* **33**, 962 (1978); A. Suzuki, H. Kyuragi, S. Matsumura, and H. Matsunami, *Jpn. J. Appl. Phys.* **19**, L207 (1980).
- <sup>29</sup>F. C. Larché and J. W. Cahn, *J. Appl. Phys.* **62**, 1232 (1987). See also F. C. Larché, W. C. Johnson, C. S. Chiang, and G. Martin, *J. Appl. Phys.* **64**, 5251 (1988).
- <sup>30</sup>M. C. Joncour, J. L. Benchimol, J. Burgeat, and M. Quilicq, *J. Phys. (Paris) Colloq.* **43**, C5-3 (1982).
- <sup>31</sup>M. H. Grabow and G. H. Gilmer, in *Initial Stages of Epitaxial Growth*, Vol. 94 of *Materials Research Society Symposium Proceedings*, edited by R. Hull, J. M. Gibson, and D. A. Smith (MRS, Pittsburgh, 1987), p. 15.
- <sup>32</sup>T. Suzuki, A. Goymo, and S. Iijima, *J. Cryst. Growth* **93**, 396 (1988).
- <sup>33</sup>D. W. Pashley, in *Layered Structures, Epitaxy, and Interfaces*, Vol. 37 of *Materials Research Society Symposium Proceedings*, edited by J. M. Gibson and L. R. Dawson (MRS, Pittsburgh, 1985), p. 67.
- <sup>34</sup>For substrate orientations other than [001], geometrical factors relate unit-cell dimensions to  $a_s$  and strain-induced distortions normal to the substrate are not strictly tetragonal (e.g., are trigonal for [111]).
- <sup>35</sup>W. A. Brantley, *J. Appl. Phys.* **44**, 534 (1973) should be consulted for the detailed dependence on orientation. The [110] case is given in Ref. 36.
- <sup>36</sup>S. Froyen, S.-H. Wei, and A. Zunger, *Phys. Rev. B* **38**, 10 124 (1988).
- <sup>37</sup>G. Simmons and H. Wang, *Single Crystal Elastic Constants and Calculated Aggregate Properties: A Handbook* (MIT Press, Cambridge, Mass., 1971).
- <sup>38</sup>J. W. Matthews, in *Dislocations in Solids*, edited by F. R. N. Nabarro (North-Holland, Amsterdam, 1979), Vol. 2, Chap. 7, p. 461.
- <sup>39</sup>B. W. Dodson and J. Y. Tsao, *Appl. Phys. Lett.* **51**, 1325 (1987); B. W. Dodson and P. A. Taylor, *ibid.* **49**, 642 (1986).
- <sup>40</sup>G. B. Stringfellow, *J. Cryst. Growth* **27**, 21 (1974).
- <sup>41</sup>J. E. Bernard, L. G. Ferreira, S.-H. Wei, and A. Zunger, *Phys. Rev. B* **38**, 6338 (1988).
- <sup>42</sup>S.-H. Wei and A. Zunger, *J. Vac. Sci. Technol. A* **6**, 2597 (1988), and unpublished.
- <sup>43</sup>B. de Cremoux, *J. Phys. (Paris) Colloq.* **43**, C5-19 (1982).
- <sup>44</sup>B. de Cremoux, P. Hirtz, and J. Ricciardi, in *GaAs and Related Compounds 1980*, *Inst. Phys. Conf. Proc. Ser. No. 56*, edited by H. W. Thim (IOP, London, 1981), p. 115.
- <sup>45</sup>R. E. Nahory, M. A. Pollack, E. D. Beebe, J. C. DeWinter, and M. Ilegems, *J. Electrochem. Soc.* **125**, 1053 (1978).
- <sup>46</sup>G. B. Stringfellow, *J. Electron. Mater.* **11**, 903 (1982); see also J. P. Hirth and G. B. Stringfellow, *J. Appl. Phys.* **48**, 1813 (1977).
- <sup>47</sup>M. Quilicq, C. Daguët, J. L. Benchimol, and H. Launois, *Appl. Phys. Lett.* **40**, 325 (1982).
- <sup>48</sup>M. Ishikawa and R. Ito, *Jpn. J. Appl. Phys.* **23**, L21 (1984).
- <sup>49</sup>W. A. Jesser and D. Kuhlmann-Wilsdorf, *Phys. Status Solidi* **19**, 95 (1967).
- <sup>50</sup>J. Cahn, *Acta Metall.* **9**, 795 (1961); **10**, 907 (1962); **10**, 179 (1962).
- <sup>51</sup>C. P. Flynn, *Phys. Rev. Lett.* **57**, 599 (1986).
- <sup>52</sup>F. C. Larché and J. W. Cahn, *Acta Metall.* **33**, 331 (1985).
- <sup>53</sup>W. C. Johnson and P. W. Voorhees, *Metall. Trans. A* **18A**, 1213 (1987); **18A**, 1093 (1987); W. C. Johnson and C. S. Chiang, *J. Appl. Phys.* **64**, 1155 (1988).
- <sup>54</sup>See *J. Cryst. Growth* **45**, 3–521 (1978) for papers related to epitaxy, including vapor- and liquid-phase epitaxy.
- <sup>55</sup>V. V. Kuznetsov, P. P. Moskvina, and V. S. Sorokin, *J. Cryst. Growth* **88**, 241 (1988).
- <sup>56</sup>F. Glas, *J. Appl. Phys.* **62**, 3201 (1987).
- <sup>57</sup>F. Glas, M. M. J. Treacy, M. Quilicq, and H. Launois, *J. Phys. (Paris) Colloq.* **43**, C5-11 (1982).
- <sup>58</sup>(a) R. Bruinsma and A. Zangwill, *Europhys. Lett.* **4**, 729 (1987); (b) *J. Phys. (Paris)* **47**, 2055 (1986).
- <sup>59</sup>G. H. Gilmer and M. H. Grabow, *J. Met.* **39**, 19 (1987); S. M. Paik and S. Das Sarma, *Phys. Rev. B* **39**, 9793 (1989).
- <sup>60</sup>(a) L. G. Ferreira, S. H. Wei, and A. Zunger, *Phys. Rev. B* **40**, 3197 (1989); (b) A. A. Mbaye, L. G. Ferreira, and A. Zunger, *Phys. Rev. Lett.* **58**, 49 (1987); (c) *Phys. Rev. B* **36**, 4163 (1987); (d) S.-H. Wei, A. A. Mbaye, L. G. Ferreira, and A. Zunger, *Acta Metall.* **36**, 2239 (1988); (e) L. G. Ferreira, A. A. Mbaye, and A. Zunger, *Phys. Rev. B* **37**, 10 547 (1988); (f) **35**, 6475 (1987).
- <sup>61</sup>J. W. D. Connolly and A. R. Williams, *Phys. Rev. B* **27**, 5169 (1983).
- <sup>62</sup>A. A. Mbaye, F. Turco, and J. Massies, *Phys. Rev. B* **37**, 10419 (1988). This approach should be contrasted with Ref. 7(a) and the present work, where it is demonstrated that  $d\Delta H_{ep}/dc = 0$  does not imply  $dE_{ep}^{(n)}/dc = 0$ .
- <sup>63</sup>J. Bellon, J. P. Chevalier, E. Augarde, J. P. Andre, and G. P. Martin (unpublished).
- <sup>64</sup>J. Van Vechten, *J. Cryst. Growth* **71**, 326 (1985).
- <sup>65</sup>S. V. Ghaisas and A. Madhukar, *Phys. Rev. Lett.* **56**, 1066 (1986).
- <sup>66</sup>See, for example, J. C. Tully, G. H. Gilmer, and M. Shugard, *J. Chem. Phys.* **71**, 1630 (1979).
- <sup>67</sup>As discussed in Refs. 7(a) and 60(c) and 60(d), in an alloy environment some equilibrium properties, e.g., volume or linear dimensions, of a cluster may differ from their values in the pure ordered compounds  $A_nB_{4-n}$ . A convenient way to account for such "alloy-induced cluster relaxation" is to permit the equilibrium lattice parameter  $a_n$  to depend on alloy composition via the substitution  $a_n(x) = a_n(x_n) + K[a_{eq}(x, T) - a_n(x_n)]$ . For a bulk alloy within the harmonic approximation it is sufficient to multiply the bulk modulus of each cluster by  $(1-K)^2$  to account for all alloy-induced cluster effects; for the epitaxial case the  $a_n(x)$  substitution must be made in all expressions where it appears quadratically. In CVM calculations the epitaxial cluster energies  $\Delta E_n$  acquire an implicit dependence on the  $\{P_n\}$  because of this relaxation. To preserve the correct definition of the chemical potential  $\mu = d\Delta F/dx$ , one must make the replacement  $\Delta E_n \rightarrow \Delta E_n + \sum_i P_i d\Delta E_i/dP_n - \sum_i \sum_n P_n P_i d\Delta E_i/dP_n$ . For the  $\text{Cu}_{1-x}\text{Au}_x$  system a value  $K = 0.20772$ , as described in Ref. 60(c), was used for both bulk and epitaxial alloys. For  $\text{GaAs}_x\text{Sb}_{1-x}$  we have taken  $K = 0$ .
- <sup>68</sup>We assume that at the global equilibrium of the tetragonal ternary compound  $c_{eq} \approx a_{eq}$ , generally a good approximation. Under epitaxial conditions we take  $a = a_{||} = a_s$  and from the curvature of  $E_{ep}(a_s)$  extract  $q$  which, together with the bulk modulus, can be solved for, e.g., for the [001] orientation, for effective values of  $C_{11}$  and  $C_{12}$ . Such a quasicubic description makes errors of order  $(C_{33}/C_{11} - 1)$ , implying energy errors of about 6% for  $\text{Ga}_x\text{In}_{1-x}\text{P}$ , as estimated from direct valence force-field calculations for this system [see Ref. 7(a)]. For ter-

- nary compounds subject to the epitaxial constraint the (1,4,6,4,1)-fold binomial distribution degeneracies [Eq. (5.11)] of  $A_{4-n}B_nC$  clusters are also broken to an extent measured by  $(C_{33}/C_{11} - 1)$ , which we thus neglect.
- <sup>69</sup>S.-H. Wei, H. Krakauer, and M. Weinert, *Phys. Rev. B* **32**, 7792 (1985).
- <sup>70</sup>P. N. Keating, *Phys. Rev.* **145**, 637 (1966); R. M. Martin, *Phys. Rev. B* **1**, 4005 (1970).
- <sup>71</sup>M. F. Grattan and J. C. Woolley, *J. Electron. Mater.* **2**, 455 (1973); *J. Electrochem. Soc.* **127**, 55 (1980). See also J. R. Pessetto and G. B. Stringfellow, *J. Cryst. Growth* **62**, 1 (1983).
- <sup>72</sup>This omitted chemical term raises the  $\Delta H_n$  with respect to the VFF values by 0.285, 0.383, and 0.274 kcal/mol for  $n = 1, 2,$  and 3, respectively. A less important error in VFF is its imperfect description of anharmonicity; this is responsible for VFF errors in the  $\Delta H_n$  of 0.11, 0.073, and 0.197 kcal/mol for  $n = 1, 2,$  and 3, respectively. The net VFF errors are thus 0.395, 0.456, and 0.471 kcal/mol for  $\text{Ga}_4\text{AsSb}_3$ ,  $\text{Ga}_2\text{AsSb}$ , and  $\text{Ga}_4\text{As}_3\text{Sb}$ , respectively.
- <sup>73</sup>See, e.g., R. Kikuchi, *J. Chem. Phys.* **60**, 1071 (1974).
- <sup>74</sup>G. P. Srivastava, J.-L. Martins, and A. Zunger, *Phys. Rev. B* **31**, 2561 (1985).
- <sup>75</sup>R. C. Heckingbottom, *J. Vac. Sci. Technol. B* **3**, 572 (1985).
- <sup>76</sup>G. B. Stringfellow, *J. Cryst. Growth* **70**, 133 (1984).
- <sup>77</sup>H. Seki and A. Koukitu, *J. Cryst. Growth* **78**, 342 (1986).
- <sup>78</sup>F. Turco, J. C. Guillaume, and J. Massies, *J. Cryst. Growth* **88**, 282 (1988); see also Ref. 62.